



Seabed mapping in the Pelagie Islands marine protected area (Sicily Channel, southern Mediterranean) using Remote Sensing Object Based Image Analysis (RSOBIA)

Sara Innangi¹ · Renato Tonielli¹ · Claudia Romagnoli² · Francesca Budillon¹ · Gabriella Di Martino¹ · Michele Innangi³ · Roberta Laterza⁵ · Tim Le Bas⁴ · Claudio Lo Iacono⁴

Received: 13 February 2018 / Accepted: 5 October 2018 / Published online: 13 October 2018
© Springer Nature B.V. 2018

Abstract

In this paper we present the seabed maps of the shallow-water areas of Lampedusa and Linosa, belonging to the Pelagie Islands Marine Protected Area. Two surveys were carried out (“Lampedusa 2015” and “Linosa 2016”) to collect bathymetric and acoustic backscatter data through the use of a Reson SeaBat 7125 high-resolution multibeam system. Ground-truth data, in the form of grab samples and diver video-observations, were also collected during both surveys. Sediment samples were analyzed for grain size, while video images were analyzed and described revealing the acoustic seabed and other bio-physical characteristics. A map of seabed classification, including sediment types and seagrass distribution, was produced using the tool Remote Sensing Object Based Image Analysis (RSOBIA) by integrating information derived from backscatter data and bathy-morphological features, validated by ground-truth data. This allows to create a first seabed maps (i.e. benthoscape classification), of Lampedusa and Linosa, at scale 1:20 000 and 1:32 000, respectively, that will be checked and implemented through further surveys. The results point out a very rich and largely variable marine ecosystem on the seabed surrounding the two islands, with the occurrence of priority habitats, and will be of support for a more comprehensive maritime spatial planning of the Marine Protected Area.

Keywords Multibeam bathymetry · Backscatter · Benthoscapes · Seabed classification · Ground-truth data · *Posidonia oceanica* · Coralligenous habitat

Electronic supplementary material The online version of this article (<https://doi.org/10.1007/s11001-018-9371-6>) contains supplementary material, which is available to authorized users.

✉ Sara Innangi
sara.innangi@cnr.it

- ¹ Istituto di Scienze Marine, CNR, Calata Porta di Massa, 80, 80133 Napoli, Italy
- ² Dipartimento di Scienze Biologiche, Geologiche ed Ambientali, Università di Bologna, Piazza di Porta S. Donato 1, 40127 Bologna, Italy
- ³ Dipartimento di Scienze e Tecnologie Ambientali, Biologiche e Farmaceutiche, Università degli Studi della Campania “Luigi Vanvitelli”, Via Vivaldi 43, 81100 Caserta, Italy
- ⁴ National Oceanography Centre, University of Southampton, Waterfront Campus, European Way, Southampton SO14 3ZH, UK
- ⁵ Senior Geophysicist, Apt 309,15, Hatton Garden, L3 2HA Liverpool, Merseyside, UK

Introduction

Marine protected areas (MPAs) play a key role in the promotion of the sustainable use of marine resources and ecological conservation (Agardy 1994). The European Framework and national laws award protect those particular areas by imposing measures to monitor the environmental status of such areas (e.g. Jameson et al. 2002; Pomeroy et al. 2005; Guidetti et al. 2008; Pieraccini et al. 2016). The Pelagie Islands marine protected area (Sicily Channel, southern Mediterranean) is characterized by different geological features (including sedimentary as well as volcanic substrate) corresponding, in association with specific biological communities, to a diversity of marine habitats. In this context, the Pelagie Islands MPA launched a project (Di Martino et al. 2015; Tonielli et al. 2016; Innangi and Tonielli 2017) to assess the conservation status and map the distribution of *Posidonia oceanica* meadows (Hemminga and Duarte 2000; Gobert et al. 2006) and coralligenous habitat (Sartoretto

1994; Barbera et al. 2003; Bonacorsi et al. 2012) This is a major issue in the context of biodiversity conservation in the Mediterranean, as highlighted in the “Action plan for the conservation of the Coralligenous and other calcareous bioconcretions in the Mediterranean Sea” (Birkett et al. 1998; UNEP-MAP-RAC 2008). Although these calcareous bioconcretions are considered well represented in the Mediterranean Sea, in fact, their precise range of distribution is not yet well known (Agnesi et al. 2009) and information commonly consist of sparse geo-referenced data on species and habitat occurrences (Martin et al. 2014). For this purpose, multibeam bathymetry and related backscatter signal are increasingly used to map benthic habitats (or *benthoscapes*, according to Lacharité et al. 2017), with the support of seafloor samples and/or photographs (e.g. Kostylev et al. 2001; Brown et al. 2011; Micallef et al. 2012; Innangi et al. 2015; Tonielli et al. 2016). In the Mediterranean these techniques are useful in determining the presence of the seagrass *Posidonia oceanica* (L.) Delile (e.g. De Falco et al. 2010; Micallef et al. 2012) and coralligenous habitats (e.g. Bonacorsi et al. 2012;

Bracchi et al. 2015, 2017). Indeed, through a qualitative and quantitative analysis of acoustic backscatter data, MultiBeam Echo Sounder (MBES) systems have been used in the last decades to infer a number of physical, geological and biological proprieties of the seafloor, such as surface roughness (e.g. Stewart et al. 1994; Fonseca and Mayer 2007; Fonseca et al. 2009), sediment grain size (e.g. Collier and Brown 2005; Bentrem et al. 2006; Lo Iacono et al. 2008; Brown and Blondel 2009), substrate type (e.g. Dartnell and Gardner 2004; Karoui et al. 2009), and distribution of seagrass meadows and other biota (e.g. Innangi et al. 2008, 2015, 2016; De Falco et al. 2010; Bonacorsi et al. 2012; Micallef et al. 2012; Bracchi et al. 2015, 2017; Tonielli et al. 2016). Moreover, it has been shown that the variation of backscatter intensity is related to sediment properties (Briggs et al. 2002; Goff et al. 2004; Parnum et al. 2005; Ferrini and Flood 2006; Sutherland et al. 2007). The aim of this paper is to create seabed maps of the insular shelf of Lampedusa and Linosa through information obtained from geophysical and ground-truth data. Moreover, we test the capability of RSOBIA (*Remote*

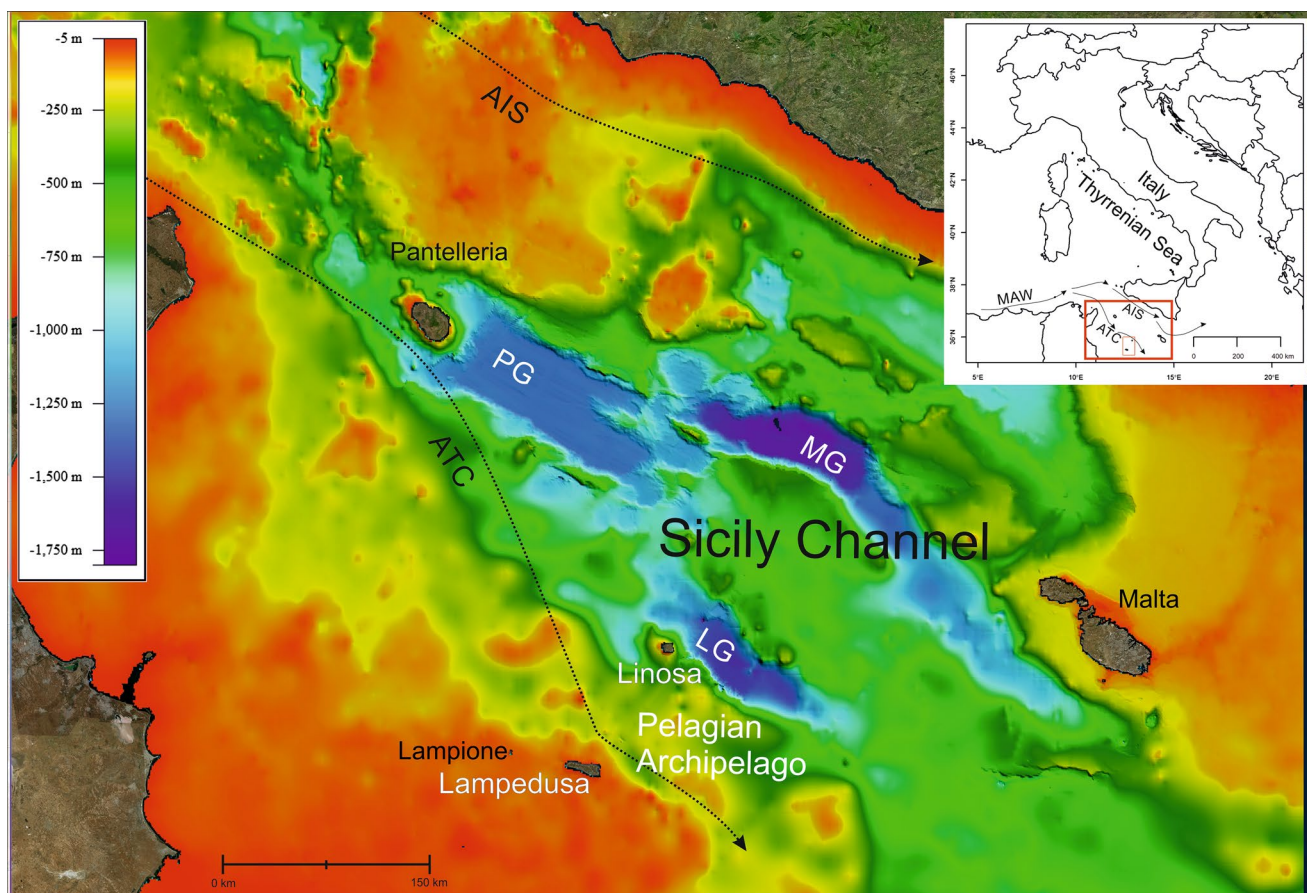


Fig. 1 Location Map of Lampedusa and Linosa islands in the Sicily Channel (Central Mediterranean Sea, Italy). Bathymetry are taken from EMODnet portal (<http://www.emodnet-bathymetry.eu/data-products>); the Pantelleria graben (PG), the Malta graben (MG), and

the Linosa graben (LG) are the principal tectonic depressions of the Sicily Channel. The Atlantic Ionian Stream (AIS) and the Atlantic Tunisia Current (ATC) (Astraldi et al. 2001; Poulain et al. 2012) are shown (The MAW flows are shown in inset)

Sensing Object Based Image Analysis; Le Bas 2016), i.e. an OBIA application integrated into ESRI's ArcMap GIS, as an objective and quantitative method to interpret geophysical data with time-savings and simplified procedures. Automated classification systems are becoming more widely used in seabed mapping due to the need for repeatable, statistically-based and unbiased procedures supporting the verification of acoustic variability in relation to seabed properties (Biondo and Bartholomä 2017). For marine benthic habitat mapping, these applications may allow the identification of homogeneous and discrete areas of the seabed characterized by different biophysical characteristics, such as bathymetry, occurrence of hard/soft substrates, sediment types and biological structures (Lacharité et al. 2017). RSOBIA, like eCognition software made by Trimble (e.g. Lucieer 2008; Diesing et al. 2014; Montereale Gavazzi et al. 2016; Lacharité et al. 2017; Ierodiaconou et al. 2018), allows to analyze acoustic backscatter mosaic and bathymetric data characteristics (i.e. depth, roughness and slope) and, through the integration with other data such as ground-truth information, provides semi-automated acoustic seabed classification of multibeam images. The produced seabed maps will thus contribute to the mapping of benthic habitat in shallow water areas around the Pelagic islands and could be of support for a more comprehensive maritime spatial planning of the Marine Protected Area. Good quality information on the spatial distribution of vulnerable species and their associated habitats is crucial for successful conservation measures and critical to decision-makers and managers (Martin et al. 2014).

Study area

The Pelagian Archipelago (Sicily, Italy) is located in the Sicily Channel (central Mediterranean Sea, Fig. 1), lying on the African lithosphere, i.e. the Pelagian Block. This was affected by crustal stretching active in the Neogene-Quaternary, giving rise to an intraplate rift system (Lentini et al. 1995; Civile et al. 2010 and references herein). The Sicily Channel is an epicontinental sea, with average depth of less than -400 m, locally interrupted by deep, tectonically-controlled, NW-SE oriented troughs (Pantelleria, Malta and Linosa grabens; Lanti et al. 1988; Grasso et al. 1991; Civile et al. 2010; Argnani 1990; Fig. 1). Anorogenic (mainly alkaline to peralkaline) volcanism of Neogene-Quaternary age is developed in correspondence of Pantelleria and Linosa volcanic edifices (Grasso and Pedley 1985; Calanchi et al. 1989). The Sicily Channel is a high-energy site with a dynamic and highly variable current system that exchanges waters between the Western and Eastern Mediterranean Basins. In particular, a water mass (about 200 m thick) of Modified Atlantic Mediterranean Water (MAW) flows eastward, (Fig. 1, inset) and, after entering the Sicily Channel, splits into two main branches, the Atlantic

Ionian Stream (AIS) and the Atlantic Tunisia Current (ATC) (Fig. 1; Astraldi et al. 2001; Poulain et al. 2012). This complex circulation patterns, together with bottom structures such as seamounts, banks, volcanoes, pockmarks and steep-walled basins, are the main factors responsible for the biodiversity richness of the Sicily Channel, where healthy deep coral communities find favorable habitat and several pelagic species such as anchovies, bluefin tuna and fin whales have spawning and feeding areas (UNEP-MAP-RAC 2015). This study focuses on Lampedusa and Linosa shallow-water marine area. Lampedusa is the largest island of the Pelagian archipelago, showing a surface area of 20 km^2 and a maximum elevation of 133 m above sea level. It is entirely made of sedimentary rocks (mainly biolites and calcarenites), ranging in age from Late Miocene to Late Pleistocene (Grasso and Pedley 1988). Linosa Island differs from Lampedusa because it is the emerging tip of a larger volcanic complex, lying on the western shoulder of the Linosa graben (Fig. 1; Grasso et al. 1991). The island shows a surface area of about 5.4 km^2 and has a maximum elevation of about 195 m above sea level. Despite their different nature, both islands show, in shallow-water, the occurrence of insular shelves covered by terraced, submarine depositional bodies. These represent a common feature on steep and narrow shelves such as on insular, volcanic or tectonically-controlled margins (Chiocci et al. 2004).

Methods

Acoustic data acquisition and processing

Geophysical data were collected by the Institute for Coastal Marine Environment of the National Research Council (IAMC-CNR) of Naples (Italy) around Lampedusa and Linosa islands down to 50 m and to 190 m of depth, respectively (see “MBES lines” in Fig. 2), during two oceanographic surveys, “Lampedusa 2015” and “Linosa 2016”. Both surveys were performed using a pole-mounted Reson SeaBat 7125 400 kHz MBES, providing sub-centimetric resolution. The vessels were equipped with an Omnistar Differential Global Positioning System (DGPS) and an IxSea Octans 3000 gyrocompass and motion sensor that provided positioning data (with sub-meter accuracy) and attitude data (0.01° accuracy). A Valeport miniSVS sound velocity probe and a sound velocity profiler were used to provide the real-time surficial sound speed for the beam steering and the velocity profile required for the depth computation. The Reson PDS2000 4.1.2.9 version was used for logging and processing MBES bathymetric data: tide data, recorded during acquisition, were applied to all dataset to set up the real depth before starting the despiking process to generate a final 2.5×2.5 m resolution grid model. Backscatter data were also collected by MBES systems as snippet data (De Falco et al. 2010; Innangi

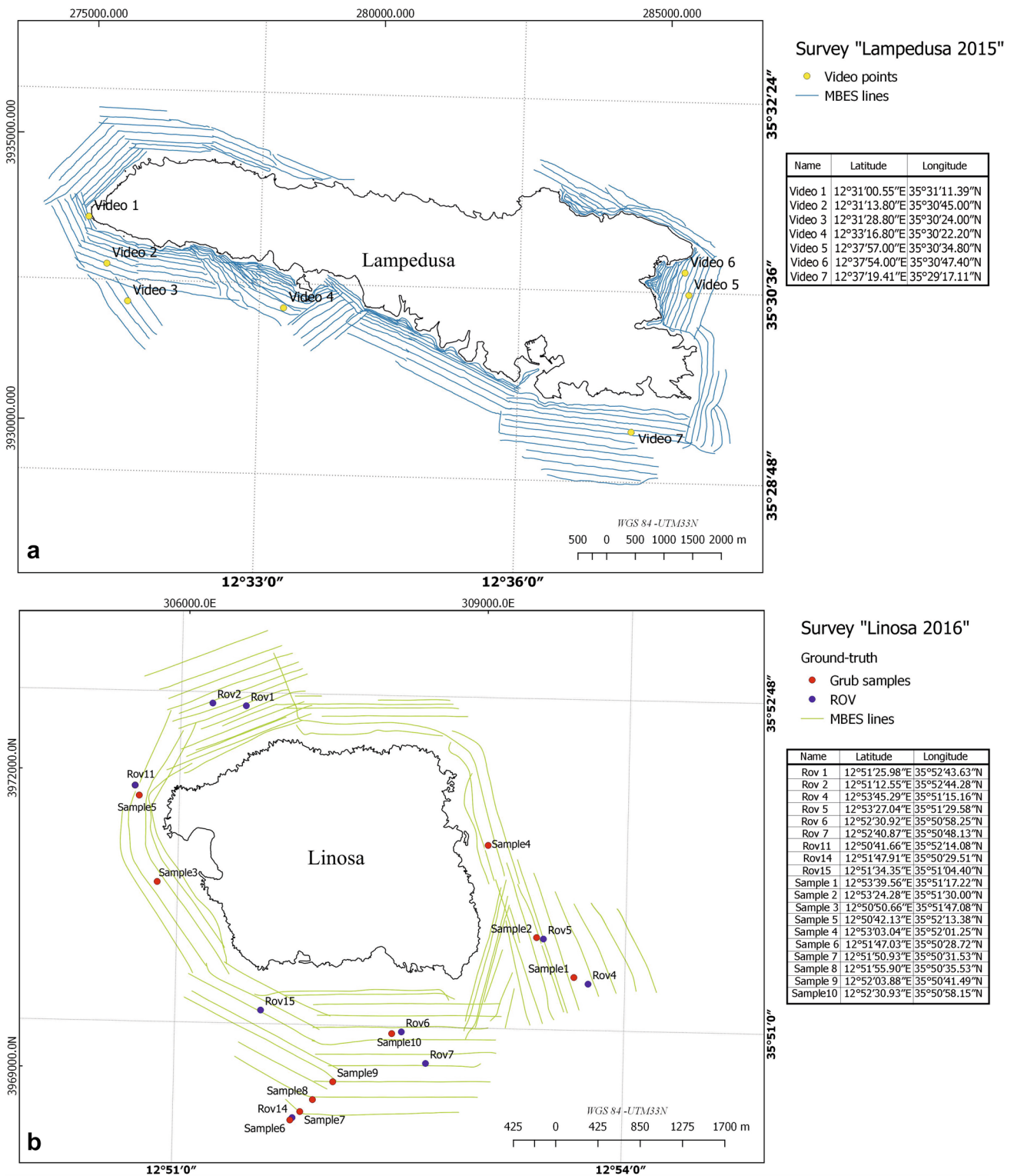


Fig. 2 **a** MBES navigation lines of the survey “Lampedusa 2015” and positions of collected underwater video inspections; **b** MBES navigation lines, positions of collected ROV inspections and grab samples of the survey “Linosa 2016”

et al. 2015). Snippet data processing was carried out using FMGeocoder Toolbox (FMGT) in Fledermaus 7.6 version (QPS 2016). These data were corrected for receiver gain,

transmit power, transmit pulse width, spherical spreading, attenuation in the water column, area of ensonification, beam pattern, speckle noise and, finally and most importantly, for

angular dependence and local slope (Mallace 2012; Fledermaus 2016). The final mosaic was exported as a geo-referenced TIFF image with a 2.5 m pixel size and imaged using a grey scale in which higher backscatter values correspond to darker areas. A range of signal values spanning from – 60 to –25 dB was adopted in the maps. The MBES used for this study was not calibrated to obtain absolute backscatter levels. Consequently, backscatter data presented are in relative (dB) units and cannot be compared with absolute values reported in other studies, as in De Falco et al. (2010). However, the backscatter facies have been locally calibrated with ground-truth information derived from sea-bottom samples and video images, enabling to infer the nature of the different substrata.

Ground-truth information

During the surveys, sea-bottom samples and video images were collected as ground-truth information. During the “Lampedusa 2015” survey, due to the boat’s limited dimension, direct assessment was carried out through video-camera inspections. A GoPro Hero 3 White camera with 1080p resolution, 5 MP photos with 3 fps burst mode with integrated flat lens housing, remotely controlled, was used. During “Linosa 2016”, both seafloor samples and direct observations were

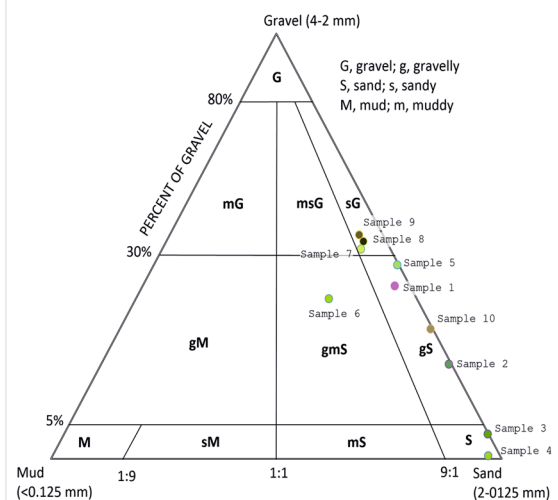
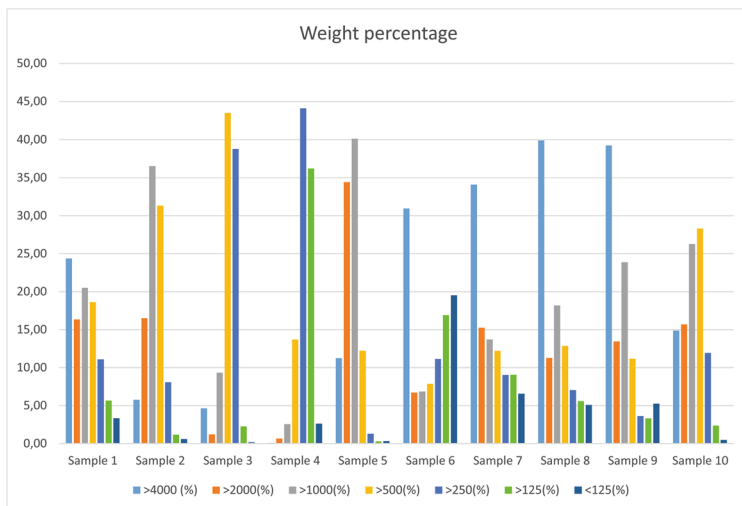
carried out by using, respectively, a Van Veen grab and a Pollux III R.O.V (Remote Operated Underwater Vehicle) equipped with two video cameras (high and low resolution). Figure 2 shows the locations and the coordinate points of the ground-truth data at Lampedusa and Linosa. Seafloor samples were photographed on deck and their lithological macroscopic features described. Then, several sub-samples were taken from the homogenized sample and grain-size analyses were performed in laboratory. The sediments were washed with hydrogen peroxide solution (30% v/v) and distilled water; the gravel/sand fraction (4–0.125 mm) was analyzed using dry sieving. Grain size fractions were classified according to the Udden-Wentworth scale (after Pettijohn et al. 1987) and according to Folk 1980 (Table 1).

RSOBIA

RSOBIA (Remote Sensing Object Based Image Analysis) application was used to segment and classify the seabed of Linosa and Lampedusa with an automatic object-based image analysis (see <https://conference.noc.ac.uk/product/rsobia-softw> are). RSOBIA is a new toolbox for ArcMap 10.4 that segments the data layers into a set of polygons. The tool operates by taking multi-layered raster imagery and segments data into

Table 1 Sediment classification according to Folk (1980) and Wentworth (1987). Left below: histograms of weight percentage of Wentworth size class. Right below: Folk’s ternary diagram

Name	Gravel (4-2mm)	Sand (2 - 0.125mm)	Silt (< 125 mm)	Folk's Classification	Wentworth's classification	Depth
Sample 1	40,73	55,91	3,36	Gravelly Sand	Coarse sand and gravel	93
Sample 2	22,29	77,11	0,60	Gravelly Sand	Coarse sand	74
Sample 3	5,88	93,93	0,19	Sand	Medium sand	54
Sample 4	0,76	96,61	2,63	Sand	Fine sand	47
Sample 5	45,68	53,99	0,33	Gravelly Sand	Very coarse sand and gravel	132
Sample 6	37,67	42,80	19,53	Gravelly muddy Sand	Very fine sand and gravel	172
Sample 7	49,36	44,06	6,58	Sandy Gravel	Medium fine sand and gravel	103
Sample 8	51,20	43,70	5,11	Sandy Gravel	Gravel and medium coarse sand	86
Sample 9	52,72	42,03	5,26	Sandy Gravel	Gravel and medium coarse sand	79
Sample 10	30,58	68,93	0,49	Gravelly Sand	Very coarse sand and gravel	40



geographic areas with similar statistical properties. Segmentation and Classification are key techniques for image analysis and this tool gives quick and easy results. Imagery derivative processing techniques are provided for ease of use but also include texture analysis techniques such as homogeneity, dissimilarity, contrast and others (Grey Level Co-occurrence Matrices—GLCMs; <https://conference.noc.ac.uk/product/rsobia-software>). In detail, segmentation is the process of partitioning a dataset into clusters of contiguous elements that are similar with respect to a range of selected parameters (Hillman et al. 2017). Each polygon is defined by K-means clustering and region-growing algorithm, for finding areas and boundaries in the imagery as well as associated mean and standard deviation of the pixel values within the polygon (Le Bas 2016; see also; Wagstaff et al. 2001; Blaschke 2010; Li et al. 2014). The attribute for each polygon can be extended with imagery attributes of pixel mean and standard deviation of each data layer, and wherever ground-truth point data is available. In this way the results from samples, where available, have been utilized to characterize the class type. The adopted segmentation process has been taken from RSGIS library of analysis and classification routines (Bunting et al. 2014), specifically modified to be suitable for the ESRI ArcGIS software under Windows operating system. The RSOBIA toolbar consists of three sections (Fig. 3), respectively designed for: (i) obtaining mathematical derivatives from a single band imagery,

such as slope maps from topography (Fig. 3a); (ii) creating polygonised feature data either by multi-band imagery, or by a combination of single layer grids making a multi-layered dataset (Fig. 3b); (iii) performing the classification and interpretation of polygonised features (further details on RSOBIA toolbar can be found in Le Bas 2016). The segmentation with RSOBIA needs the definition of three main parameters: *Number of Clusters*, *Minimum Object Size* (the minimum size of any output polygon in terms of pixels, that is the resolution) and *Layer Weights* (Fig. 3c). In this study, for both islands, we adopted 10 as the number of clusters, as it was shown to be the optimal number of clusters after several trials, and 20,000 as object size, in relation to the map scale. We decided to run a preliminary test on the segmentation procedure based on the study by Lacharité et al. (2017), which used backscatter (Fig. 4a) and depth (Fig. 4b) data layers (BD), from snippet and bathymetry multi-layered raster, where the former was assigned twice the weight than the latter in order to prioritize substrate composition rather than local variability in depth. Given the geological and morphological differences of the seabed between the two islands object of this study, we decided to test a second, customized segmentation based on backscatter, depth, roughness (Fig. 4c) and slope (Fig. 4d) data layers (BDRS), the first one three times the weight of the others. Such segmentation is intended to also include DTM-derived variables (such as slope and roughness), however enhancing the

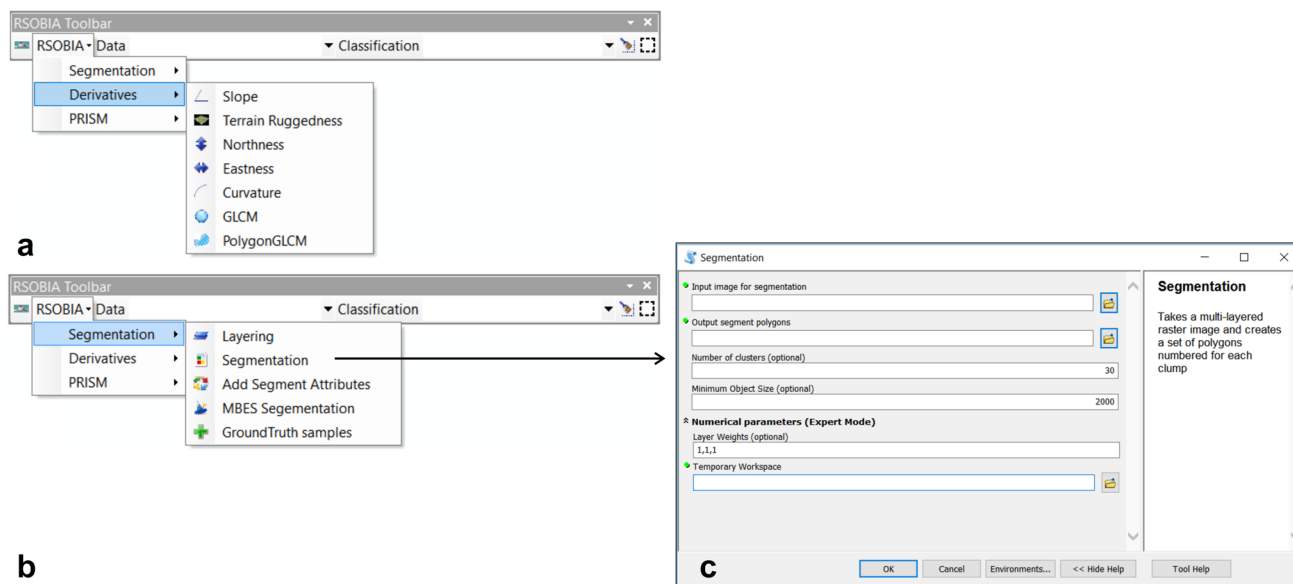


Fig. 3 RSOBIA toolbar showing both the derivatives (a) and the segmentation (b) sub-menu. In (c) is shown the Segmentation window; during the standard segmentation process each layer is given equal weighting regardless of the differing units used on each layer. The user can provide individual layer weights if, for example, one layer is deemed to provide more important or better imagery. The derivatives functions are standard grid manipulation techniques; in this study we used slope and roughness functions; the first calculates the maximum

slope (in any direction) in degrees and values created are real numbers between 0.0 and 90.0 but values of -1.0 is used for areas of no data. This function differs from a shaded relief which is a slope derivative from particular direction. For roughness, the function calculates the variations in bathymetry datasets within a neighborhood. This technique combines the variability of slope and aspect in a sampled area, similarly to the “Benthic Terrain Modeler” developed by Shaun Wallbridge (Wright et al. 2012; Le Bas 2016)

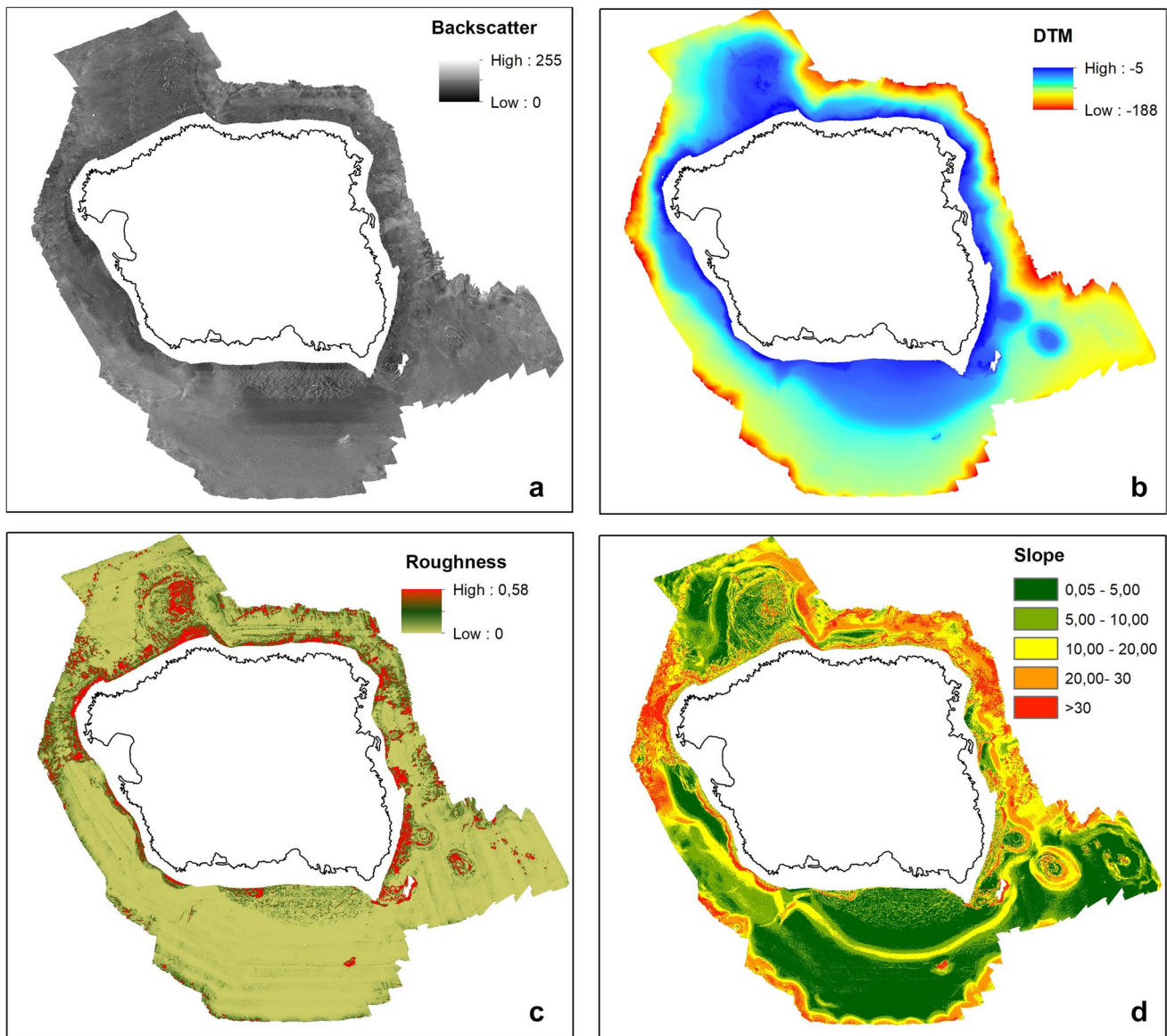


Fig. 4 Raster images used to analyze the Linosa seabed with RSOBIA. **a** Snippet mosaic (backscatter), with brightness values are indicated (low value corresponding to high backscatter and low

absorption); **b** DTM image (in meters); **c** the surface roughness (in dimensionless value) derived through RSOBIA; **d** the slope image (in degree) derived through RSOBIA

role of backscatter signal by increasing its importance in the segmentation. Hereafter we will refer to these two segmentation approaches as *BD* and *BDRS*, respectively.

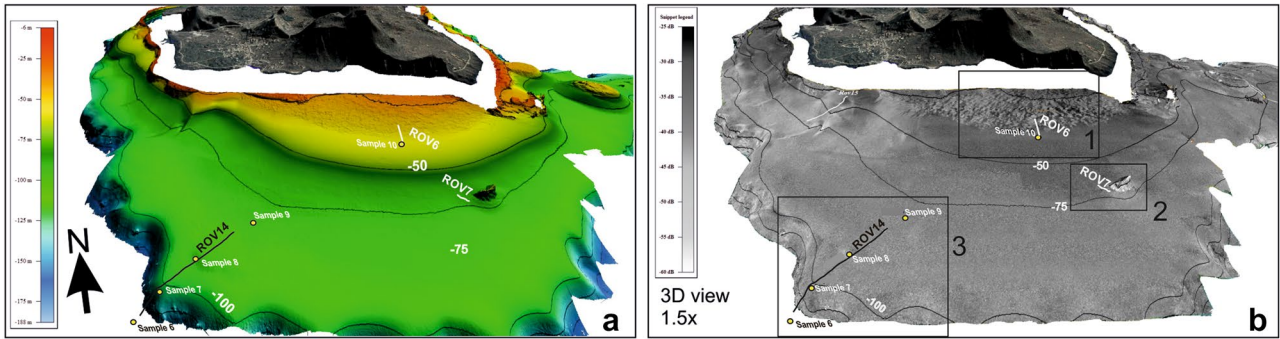
Results

Seabed characteristics

Linosa

The DTM of Linosa shows an articulated morphology, dominated by the occurrence of well-developed insular

shelves down to about 100–120 m depth, all around the SW-S-SE sectors and offshore the NW of the island (see Fig. ESM1A). The resulting backscatter mosaic of Linosa Island (Fig. ESM1B) does not show a high variability of the acoustic facies, probably due to the nature of the volcanic substratum, that tends to oversaturate the acoustic signal, and of the overlying deposits. In detail, the southern insular shelf (Fig. 5) has a sub-rounded shape and extends for over 1.5 km from the coastline seaward, with an average slope of 3° . It is characterized by two main slope breaks, at depth of around 45/50 m and 90/100 m (section T'1 in Fig ESM1A), that correspond to the outer edge of two prograding terraced depositional bodies, lying

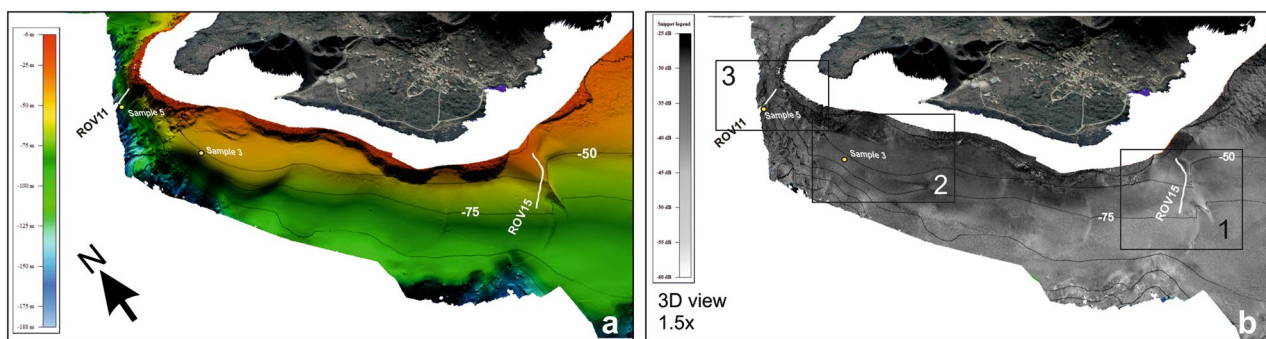


DTM	Backscatter	ROV video frame	Sample	Physical parameters	Seabed composition
Sector 1 in map					
				Intermediate backscatter pattern interrupted by elongated patches of high backscatter. Low slope (~ 1.8°)	Volcaniclastic and bioclastic coarse sand covered by dense patches of <i>P. oceanica</i> .
				Homogeneous pattern of high backscatter. Low slope (~ 1.8°)	Volcaniclastic and bioclastic coarse sand and gravel interspersed with maërl
Sector 2 in map					
				Homogeneous pattern of medium/low backscatter. Low slope (~ 1.8°)	Rhodolith and maërl beds interspersed with bioclastic coarse sand and gravel.
Sector 3 in map					
				Homogeneous pattern of medium/low backscatter. High slope (~ 33°)	Bioclastic very fine sand and gravel.
				Homogeneous pattern of medium/low backscatter. High slope (~ 33°)	Bedrock covered by dense coralligenous concretions. Bioclastic medium fine sand and gravel.
				Homogeneous pattern of medium/low backscatter. Medium/high slope (~ 5°–10°)	Bioclastic medium/coarse sand covered by dense <i>Lhytophyllum</i> and rhodolith beds
				Homogeneous pattern of medium/low backscatter. Low slope (~ 0.60°)	Bioclastic medium/coarse sand covered by dense <i>Lhytophyllum</i> and rhodolith beds

Fig. 5 Bathymetry (a) and backscatter (b) 3D visualization of the southern part of Linosa. Follow shaded relief, backscatter imagery, ROV video frame, samples' photos, description of physical parameters and seabed composition of three sector investigated in this area of Linosa. See the text for details

on the inner part and at the edge of the insular shelf, respectively (Romagnoli 2004). In this sector, between –20 and –30 m depth range, an irregular pattern is evident, both in morphology and in backscatter data. In particular, the acoustic mosaic shows an intermediate backscatter interrupted by elongated patches of higher backscatter (ranging in values from –55 to –35 dB). This speckled pattern is interpreted as due to irregular *P. oceanica* meadows (similarly to what was indicated for the Malta offshore by Micallef et al. 2012). This hypothesis was confirmed by the ROV 6 video images collected at around –33 m (Fig. 5, sector 1), showing the seagrass organized in dense patches that cover volcanoclastic and bioclastic coarse sand. Ground-truth data acquired in this sector, below the lower limit of *P. oceanica* (at about 38–39 m depth), confirm that the observed more homogeneous seabed pattern with high backscatter signal, corresponds to coarse volcanoclastic sand and gravel interspersed with maërl (see Sample 10 in Fig. 5 and in Table 1). Moving down to 50 m depth (i.e. below the edge of the shallow-water depositional terrace, see transect T'1 in Fig. ESM1A), more regular acoustic facies occur, with medium–low backscatter (–45/–48 dB), likely corresponding to a finer-grained sedimentary cover on the seabed. The ROV 7 video images (Fig. 5, sector 2), acquired near a small morphological high, show the presence of widespread rhodolith and maërl beds (Barbera et al. 2003; UNEP-MAP-RAC 2008; Martin et al. 2014) interspersed with bioclastic coarse sand and gravel. ROV14, carried out at the end of transect T'1 (Fig. ESM1A) on the outer shelf, in an area characterized by homogeneous pattern of medium/low backscatter (–45/–50 dB, Fig. ESM1A), showed particularly well-developed Mediterranean coralligenous assemblages in natural conditions (Laborel 1961; Ballesteros 2006; UNEP-MAP-RAC 2008; Bonacorsi et al. 2012), hereafter described according to the video acquisition (i.e. moving upslope from 150 m to 80 depth Fig. 5 sector 3). Medium to fine bioclastic sand and mud are present on the seabed at –150 m (sample 6 in Fig. 5, sector 3 and in Table 1); subsequently, along the ROV transect, the volcanic bedrock is covered by increasing coralligenous concretions (at –135 m, Fig. 5, sector 3). At about 100–85 m depth the *Lithophyllum stictaeforme* (Areschoud) Hauck and coralligenous assemblages appeared to increase in size proportionally with decreasing depths (see samples 7 and 8 in Fig. 5 sector 3). At about 83–80 m depth (Rov14 video frame and sample 9 in Fig. 5, sector 3), a coral community

organized in small banks with sponges, hydrozoans, bryozoans, serpulids, echinoderma, tunicates, and other organisms was recognized (see also Pérès and Picard 1964; Laborel 1987; Ballesteros 2006). Moving westwards, in the area offshore the Linosa village, ROV 15 was acquired between 30 and 70 m depth range (Fig. 6, sector 1). A relatively homogeneous pattern of intermediate backscatter (with slightly higher values, –45 dB, at shallow depth and lower values, –35 dB, at increasing depth) corresponded, on ROV images, to a mixture of medium-coarse bioclastic (predominant at –70 m) and volcanoclastic (predominant at –30 m) sands. In shallow water (–30 m) a few specimens of *P. oceanica* are also present on the seabed. No grab samples are available for this transect. Most of the submarine western flank of Linosa shows, down to –80/90 m, a higher backscatter value (about –35 dB) compared to surrounding areas (see Fig. ESM1B). Sample 3 (Table 1), collected at –53 m on this acoustic facies is made of volcanoclastic medium sand (Fig. 6, sector 2). More to the north-west, images from ROV 11 and Sample 5 at about 130 m depth show the occurrence of bioclastic very coarse sand (Fig. 6, sector 3) with scattered rhodoliths/maërl and, at shallower depth (–80 m), abundant encrusting organisms on bedrocks (Fig. 6, sector 3). Off the northern coast of Linosa, a NNW-SSE oriented insular shelf develops for over 1 km far from the island, corresponding to the Secca di Tramontana shoal (Fig. ESM1A and Fig. 7). It partly corresponds to the remnant of a largely dismantled eruptive center located to the N of the island (Lanti et al. 1988; Lanzafame et al. 1994). The flanks of Secca di Tramontana appear to be asymmetric, with a steeper eastern side (about 25°) affected by a wide scar corresponding to a canyon head (Romagnoli 2004) and a less steep (5° on average) terraced western flank (transect T'2 in Fig. ESM1A). On the Secca di Tramontana shoal the seabed shows high backscatter values at the top (ranging from –35 to –30 dB at around 20–25 m depth), probably due to the high reflectivity of the bedrock, which by far corresponds to the main component of the backscatter strength. Two ROV video-inspections were carried out on the western side of the shoal to determine the *P. oceanica* extension. ROV 1 at 25 m depth and ROV 2 at 28 m depths showed well-developed and dense *P. oceanica* meadows lying on a rocky substrate (Fig. 7, sector 1) while, both at lower (–20 m) and higher (–48 m) depth, *P. oceanica* is absent, except for scattered tufts, while photophilic algae predominate (Fig. 7, sector 1 and sector 2). The NE and E submarine flanks of Linosa are quite steep (slope between 14 and 25°) and affected by active gullies and canyon heads also in shallow water, due to the lack of well-developed insular shelf here (except in the sector SE of the island; Fig. ESM1A). Backscatter in these areas is mainly high, with alternating, local



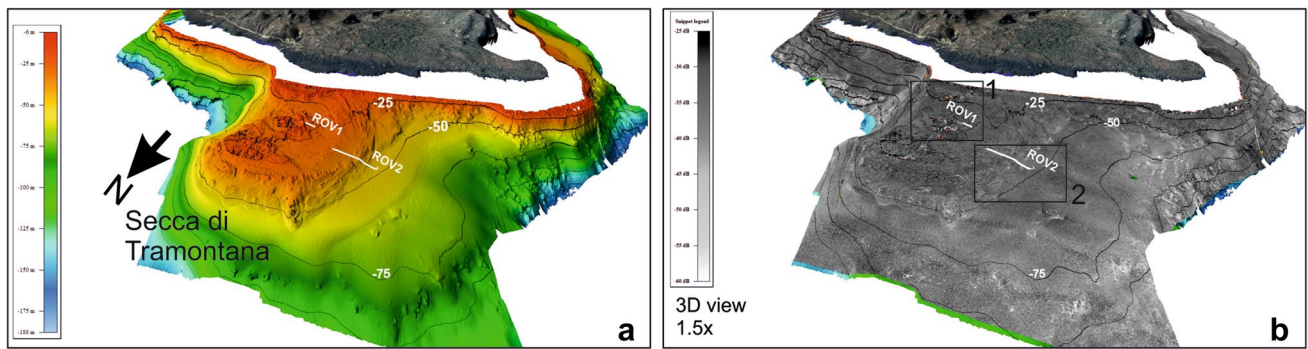
DTM	Backscatter	ROV video frame	Sample	Physical parameters	Seabed composition
Sector 1 in map					
			/	Homogeneous pattern of intermediate backscatter. Intermediate slope (~ 6°)	Bioclastic and volcanoclastic medium/coarse sand
				Homogeneous pattern of intermediate/high backscatter. Low slope (~ 1.8°)	Volcanoclastic and bioclastic medium/ coarse sand and few specimens of <i>P. oceanica</i> .
Sector 2 in map					
		/		Homogeneous pattern of high backscatter. intermediate slope (~ 8°)	Volcanoclastic medium sand.
				Homogeneous pattern of high backscatter. High slope (~ 32°)	Maërl interspersed with bioclastic very coarse sand and gravel.
Sector 3 in map					
			/	Homogeneous pattern of high backscatter. High slope (~ 32°)	Bedrock covered by dense biocostraction and coralligenous concretions.

Fig. 6 Bathymetry (a) and backscatter (b) 3D visualization of the western part of Linosa. In the columns below, shaded relief images from DTM, backscatter imagery, ROV video frame (where available),

samples’ photos (where available), description of physical parameters and seabed composition of three investigated sector are reported. See the text for details

low-backscatter areas (Fig. ESM1B). Sample 4 was collected in one of the clearer acoustic facies visible in this sector (about -58 dB; Fig. 8, sector 1), indicating the occurrence of mainly bioclastic fine sand with a limited volcanic fraction. In the SE sector, the shelf extends with a ENE-WNW elongated shape for about 1.7 km from the island. On its surface, some erosional remnants can be observed among which, in particular, two flattened and

strongly eroded sub-conical eruptive centers, each around 160 m in diameter (Fig. ESM1A and Fig. 8, sector 2 and 3). These two dismantled volcanic cones show concentric summit features (erosional remnants) and are characterized by intermediate backscatter values (-50 to -45 dB). On the eastern volcanic cone at about 100 m depth, ROV 4 showed a seabed covered by coralline alga *Lithophyllum stictaeforme* and other calcareous-coral algae (Fig. 8,



DTM	Backscatter	ROV video frame	Physical parameters	Seabed composition
Sector 1 in map				
			Homogeneous pattern of high backscatter. Low slope (~ 3°)	Bedrock covered by dense <i>P. oceanica</i> meadows
			Homogeneous pattern of high backscatter. Low slope (~ 3°)	Bedrock covered by photophilic algae and tuft of <i>P. oceanica</i>
Sector 2 in map				
			Homogeneous pattern of high backscatter. Low slope (~ 2.5°)	Bedrock covered by photophilic algae
			Homogeneous pattern of high backscatter. Intermediate slope (~ 5°)	Bedrock covered by dense <i>P. oceanica</i> meadows

Fig. 7 Bathymetry (a) and backscatter (b) 3D visualization of the northern part of Linosa. In the columns below, shaded relief from DTM, backscatter imagery, ROV video frame, description of physi-

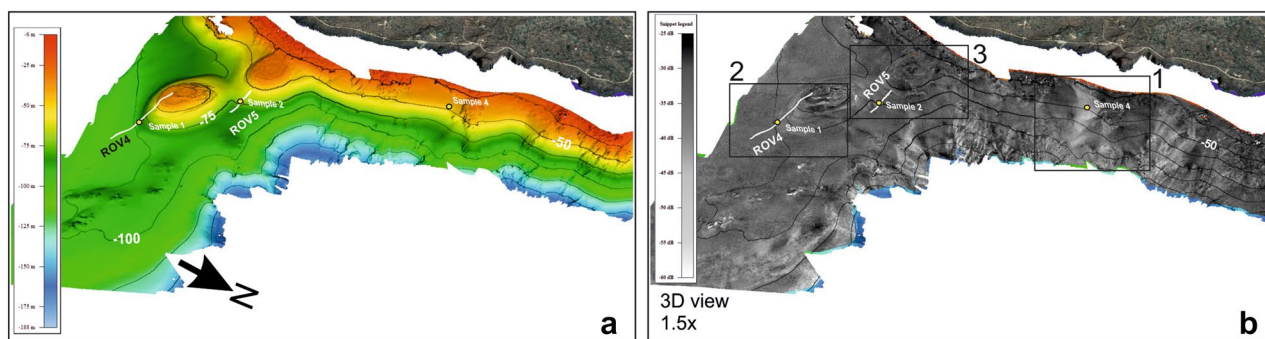
cal parameters and seabed composition of two investigated sectors of Linosa are reported. See the text for details

sector 2). Moving upslope, from about 95–90 m to 50 m depth, well-developed rhodolith beds completely cover the underlying substrate made of bioclastic and volcanoclastic coarse sand (Sample 1 in Fig. 8, sector 2 and Table 1), while at the end of the video acquisition (depth around 33 m), a rocky substrate, covered with photophilic algae, was observed on the top of the volcanic cone (corresponding to a speckled, intermediate backscatter pattern; Fig. 8, sector 2). Similarly, ROV 5 surveyed the characteristics of the seabed close to the western cone and on its top, starting at – 88 m (Fig. 8, sector 3). Here the video images showed dense rhodolith beds as well, decreasing with depth and replaced upslope by mærl beds and coarse

volcanoclastic sands (Sample 2 in Fig. 8, sector 3 and Table 1). In turn, mærl disappears at around – 50 m, where a rocky substrate covered with photophilic algae can be found.

Lampedusa

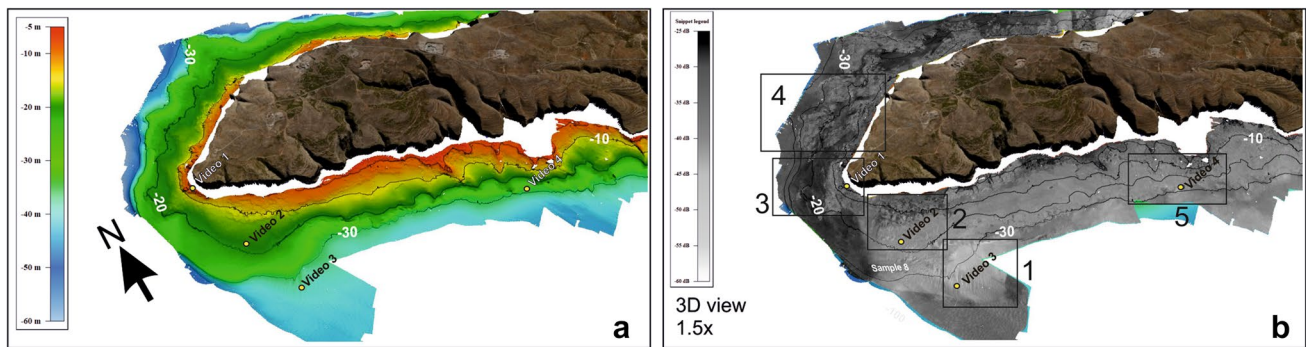
The high-resolution DTM of Lampedusa (depth range of 2–50 m, Fig. ESM2A) shows a rugged seafloor all around the island within the first 20–40 m depth, due to extensive rocky outcrops, localized talus deposits and relict morphologies on the seabed, as *P. oceanica* meadows on ‘matte’ facies (as defined by Francour et al. 2006; see Fig. es ESM2A and



DTM	Backscatter	ROV video frame	Sample	Physical parameters	Seabed composition
Sector 1 in map				Homogeneous pattern of low backscatter. Intermediate slope (~ 6°)	Bioclastic fine sand
Sector 2 in map				Homogeneous pattern of intermediate backscatter. Low slope (~ 2.5°)	Bioclastic sand covered by dense <i>Lhytophyllum</i> and rhodolith beds
				Homogeneous pattern of intermediate backscatter. Intermediate slope (~ 5°)	Bioclastic and volcanoclastic coarse sand covered by dense rhodolith beds
				Speckled pattern of intermediate backscatter. Low slope (~ 1°)	Bedrock covered by photophillic algae
Sector 3 in map				Homogeneous pattern of intermediate backscatter. Intermediate slope (~ 4°)	Bioclastic and volcanoclastic sand covered by dense rhodolith beds
				Homogeneous pattern of intermediate backscatter. Intermediate/high slope (~ 14°)	Bioclastic and volcanoclastic coarse sand and maërl
				Homogeneous pattern of intermediate backscatter. High slope (~ 22°)	Bedrock covered by photophillic algae

Fig. 8 Bathymetry (a) and backscatter (b) 3D visualization of the eastern part of Linosa. In the columns below, shaded relief from DTM, backscatter imagery, ROV video frame (where available), sam-

ples' photos (where available), description of physical parameters and seabed composition of three investigated sectors of Linosa are reported. See the text for details



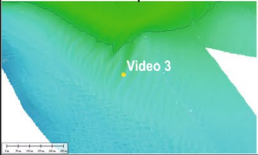
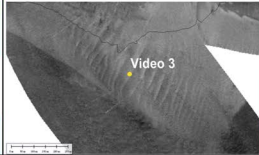
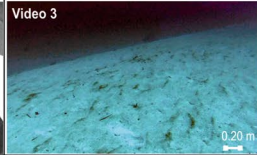

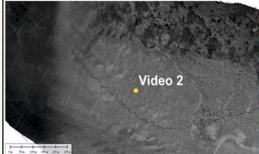
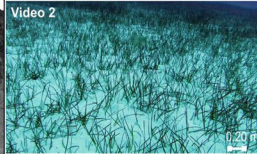
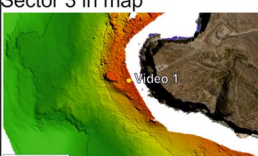
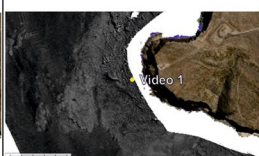
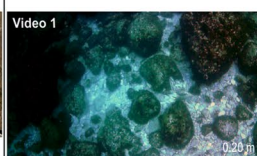
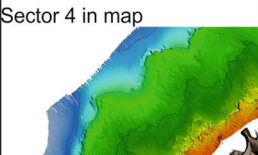
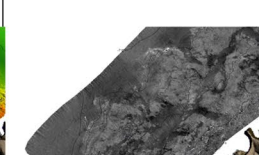
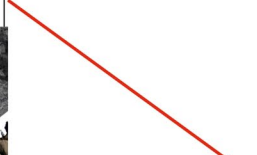
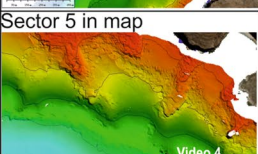

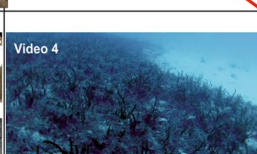
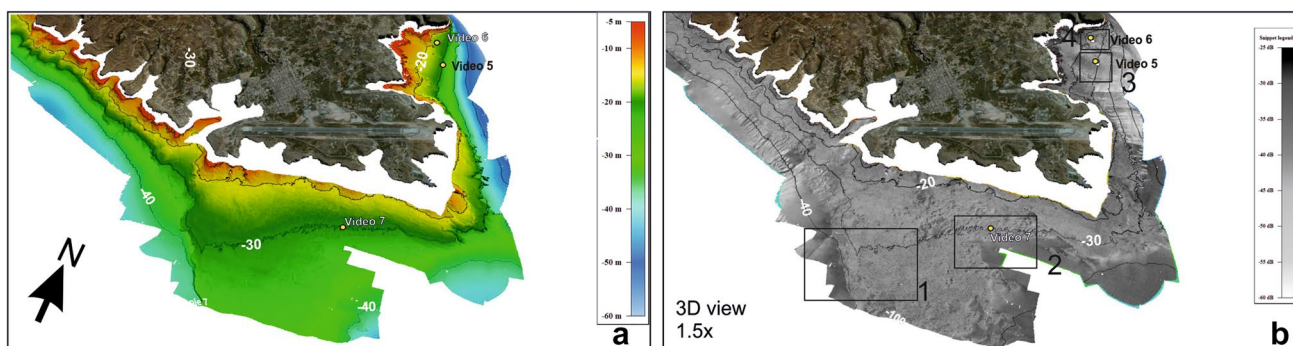
DTM	Backscatter	GoPro video frame	Physical parameters	Seabed composition
Sector 1 in map 		Video 3 	Dune field with NE-SW oriented crests. Low to high backscatter interrupted by a homogeneous pattern of high backscatter. Low slope (~ 0.5°)	Undulating and irregular seabed covered with soft sediments, likely composed of medium-fine sand.
Sector 2 in map 		Video 2 	Irregular seafloor with shortly spaced v-shaped furrows. Medium backscatter interrupted by an irregular pattern of high backscatter. To the left, homogeneous pattern of high backscatter. Low slope (~ 0.5°)	Sandy seabed covered by an irregular pattern of <i>Cymodocea nodosa</i> .
Sector 3 in map 		Video 1 	Rugged seabed of a terraced deposit at the foot of the submerged cliff. Speckled pattern of medium backscatter interrupted by homogeneous pattern of high backscatter. Medium slope (~ 3.5°)	Very coarse, heterogeneous materials, as well-rounded pebbles and boulders on poorly sorted gravel.
Sector 4 in map 			Below the coast, rugged seabed of a terraced deposit at the foot of the submerged cliff. Intermediate backscatter pattern interrupted by large pattern of high backscatter. Medium slope (~ 2°)	Likely substratum with coarse-grained sediment covered by an irregular pattern of <i>Posidonia oceanica</i> .
Sector 5 in map 		Video 4 	Homogeneous intermediate backscatter pattern interrupted by circular pattern of high backscatter. Low slope (~ 0.5°)	Superficially coarse sand to fine sand covered by dense <i>Posidonia oceanica</i> , that stops at about 38 m depth.

Fig. 9 Bathymetry (a) and backscatter (b) 3D visualization of the western part of Lampedusa. In the columns below, shaded relief from DTM, backscatter imagery, GoPro video frame (where avail-

able), description of physical parameters and seabed composition of five investigated sectors of Lampedusa are reported. See the text for details

B). Locally, vertical scarps 10–20 m high are present, such as in the eastern and northern shallow-water sectors. As recognizable on morphological sections (see Fig. ESM2A), the shallow water areas have different characteristics. Along the northern coast of the island the seabed is steeper (3.80° on average) (see Fig. 4 in Tonielli et al. 2016) and dips down to over – 50 m. Conversely, along the southern sector of the

island, the seabed slopes with a gradually decreasing gradient (about 1.80° on average) in the depth range of 10–50 m. In the SW and SE sectors, in particular, gently-sloping, terraced morphologies extend from the coast seaward (with average slope of 1.20° to 0.7°, respectively; see bathymetric transects T1 and T2 in Fig. ESM2A). This setting is due to both the geological structure of the island (see Grasso and Pedley



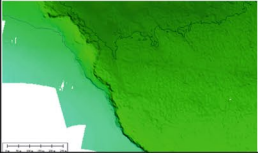
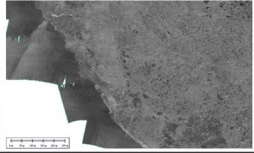
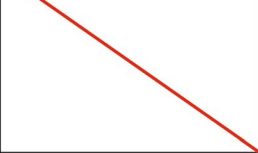

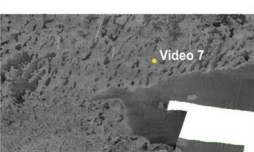



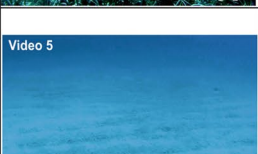
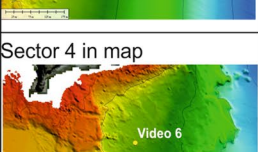

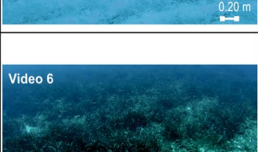
DTM	Backscatter	GoPro video frame	Physical parameters	Seabed composition
Sector 1 in map 			Rugged seafloor with intermediate backscatter pattern interrupted by elongated patches of high backscatter. Beyond 40 m depth, flat seafloor with high backscatter pattern. Low slope (~ 1.8°)	Superficially coarse sand covered by dense patches of <i>Posidonia oceanica</i> meadows.
Sector 2 in map 		Video 7 	Rugged seafloor with intermediate backscatter pattern interrupted by elongated patches of high backscatter. Beyond 30 m depth, flat seafloor with high backscatter pattern. Low slope (~ 0.4°)	Superficially coarse sand covered by dense patches of <i>Posidonia oceanica</i> meadows.
Sector 3 in map 		Video 5 	Flat seafloor with homogeneous pattern of high to intermediate backscatter. Medium slope (~ 3.2°)	Superficially coarse/medium sand.
Sector 4 in map 		Video 6 	Rugged seafloor with speckled pattern of intermediate backscatter. Beyond this facies, flat seafloor with alternate low and high backscatter. Low slope (~ 1.5°)	Bedrock with dense seagrass cover.

Fig. 10 Bathymetry (a) and backscatter (b) 3D visualization of the sud-estern part of Lampedusa. In the columns below, shaded relief from DTM, backscatter imagery, GoPro video frame (where avail-

able), description of physical parameters and seabed composition of four investigated sectors of Lampedusa are reported. See the text for details

1985) and the occurrence of erosive-depositional features, such as erosive surfaces and overlying sedimentary bodies. As showed for the island of Linosa, the acoustic backscatter mosaic is made up by the range of signal values ranged from -60 dB (lighter tones, corresponding to low backscatter) to -25 dB (dark grey tones, considered as high backscatter). Direct inspections with GoPro Hero 3, located in selected sites (Fig. 2a and Fig.es ESM2A and B) allowed to locally calibrate some of the acoustic facies in the southern and eastern submarine areas around Lampedusa and to better define some specific seabed features. In detail, Fig. 9 shows the bathymetry and the acoustic (backscatter) facies of the SW

terrace (morphological transect T1 in Fig. ESM2A). In the deeper, gently-sloping area at about 30/40 m depth, characterized by alternating low (-55/50 dB) and high (-40 dB) acoustic backscatter, local bathymetric irregularities were observed on the seabed. These corresponded to a dune field (area of 0.22 Km²), with NNE-SSW oriented asymmetric crests, wavelength between 25 and 50 m and a maximum height of about 2 m (Tonielli et al. 2016). Video 3 was recorded on the dune field, to verify the presence of maërl or rhodoliths as reported by Di Geronimo and Giaccone 1994 (see also Giardina and De Rubeis 2012). The ROV images (Fig. 9, sector 1) showed an undulating and irregular seabed

covered with soft sediments, likely composed of medium-fine sand. Given the limited resolution of the images, we were unable to verify the presence of maërl or rhodoliths on the seabed. Moving upslope on the SW terrace, video 2 (Fig. 9, sector 2), recorded at a depth ranging between 10 and 38 m, in correspondence of an irregular seafloor with shortly spaced, v-shaped furrows and with variable backscatter, the presence of *Cymodocea nodosa* (Ucria) Aschers was revealed on a sandy seabed. Close to the SW edge of the island, video number 1 (Fig. 9, sector 3) allowed to check the nature of the rugged seabed and the speckled acoustic facies observed in very shallow water, between 5 and 10 m depth. Here the occurrence of very coarse, heterogeneous materials (well-rounded pebbles and boulders) on poorly sorted gravel is observed, at the foot of the submerged cliff. On the western flank (Fig. 9, sector 4) the acoustic facies was spotted, presumably indicating an irregular substratum with coarse-grained sediment (characterized by backscatter values of -30 to -25 dB) covered by *P. oceanica* (corresponding to lower backscatter values of about -40 dB). Due to adverse weather conditions, it was not possible to acquire video images in this sector, but the occurrence of *Posidonia* is supported by previous Authors (see Tonielli et al. 2016 and references therein) and the interpretation of similar acoustic facies (see also Micallef et al. 2012; Truffarelli et al. 2012). *P. oceanica* meadows on ‘matte’ facies was present, instead, offshore the southern sector of the island, where backscatter pattern showed circular areas values with a more homogeneous, intermediate pattern (Fig. 9, sector 5; see Innangi et al. 2015 for ‘matte’ description). Video 4 allowed to check the lower limit of the *P. oceanica* meadows that here gradually thin

out, both in terms of density of leaves and height, at about 38 m depth on a sandy seafloor (Fig. 9, sector 5). Offshore the SE part of the island a NNW-SSE oriented, 4–6 m-high scarp delimited the SE terraced sector westward between 30 and 50 m of depth and corresponded to a morphological step (Fig. 10, sector 1 and T2 transect in Fig. ESM2A), in agreement with the main structural lineaments recognized on the island (Grasso and Pedley 1985). The rugged seafloor and irregular acoustic facies with intermediate backscatter (values around -45 dB) and elongated patches of high backscatter, characterizing this area down to $-30/-40$ m, is due to the presence a well-developed *P. oceanica* meadow, as confirmed by video 7 (Fig. 10, sector 2). In deeper areas, a relatively flat seabed with a high backscatter pattern occurs. Finally, offshore the eastern flank of Lampedusa, in correspondence of a large and irregular embayment, the seabed is characterized by large variation in the backscatter signal, probably due to the occurrence of sedimentary flows down the submarine flank (Fig. ESM2B). Video 5 (Fig. 10, sector 3) and 6 (Fig. 10, sector 4) were both recorded in this area: Video 5, from a low-gradient area at depth of 30 m on a medium/high backscatter patch, documents the absence of any seagrass on the medium-coarse sand covered seabed, while video 6 at around 25 m depth revealed well-developed and dense *P. oceanica* meadows over a rocky bottom characterized by speckled backscatter pattern.

Results of RSOBIA

According to the segmentation approach adopted to analyze the seabed at Linosa through RSOBIA (“RSOBIA”

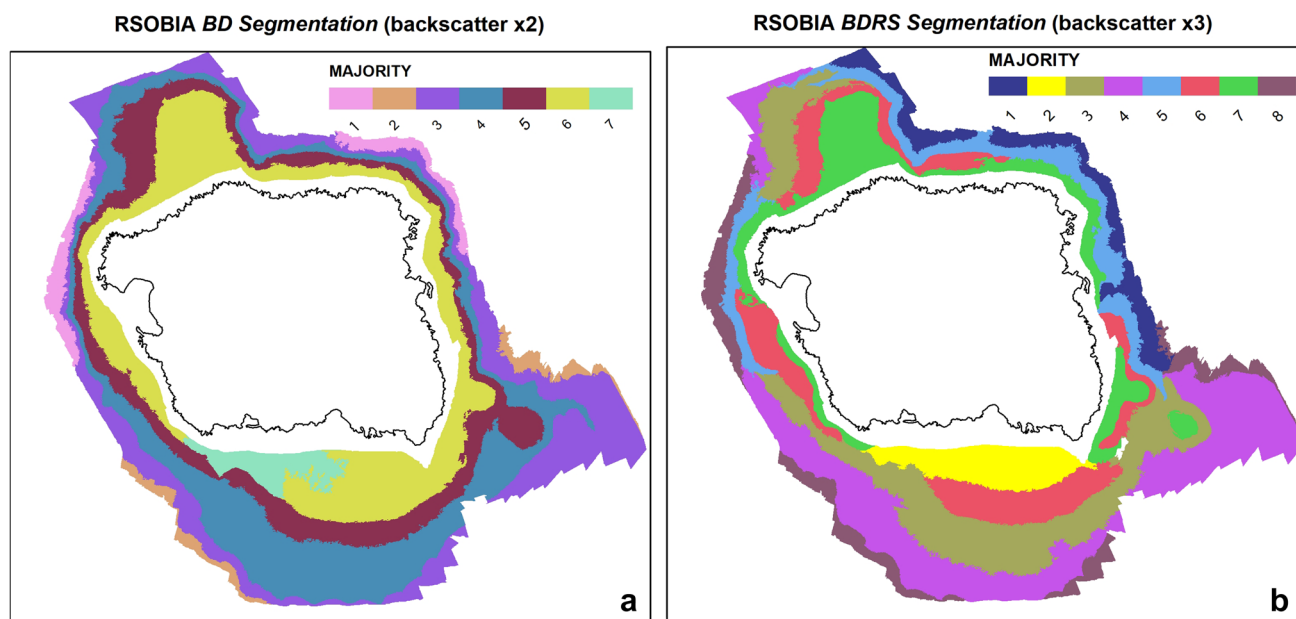


Fig. 11 RSOBIA segmentation results: **a** from BD segmentation; **b** from BDRS segmentation and related Majority class

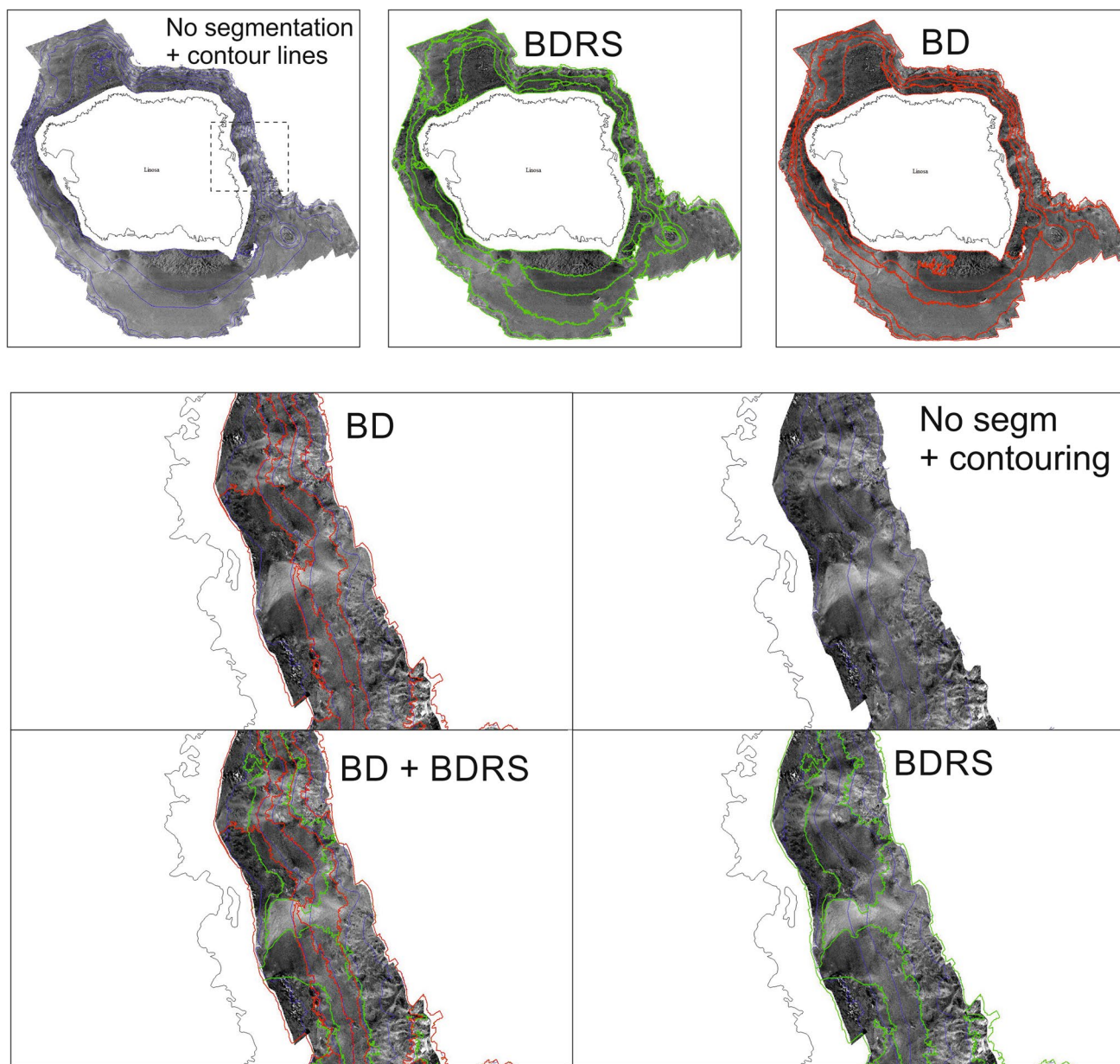


Fig. 12 Pairwise comparison of the two adopted segmentations for a sector of Linosa. BD and BDRS segmentations offers comparable results, though BD less sensitive to local facies variations. Furthermore, the BD segmentation is comparable to a simple contouring of isobaths

section and Fig. 4 for derivatives), two different results were obtained for the BD and BDRS segmentations (Fig. 11a, b, respectively). A similar approach was followed to analyze the Lampedusa data with RSOBIA (see ESM3.1 and ESM3.2). A pairwise comparison of the two adopted segmentations for a sector offshore Linosa can be seen in Fig. 12 (and in ESM3.3 for Lampedusa). It showed that BD (in red) and BDRS (in green) segmentations offer comparable results, although BD is less sensitive to local facies variations and, at Linosa, it is comparable to a simple contouring of isobaths (Fig. 11a). Accordingly, it was preferred

to apply the BDRS segmentation (see “RSOBIA” section). The differences obtained between the two segmentations at Linosa are likely related to the fact that, given its volcanic nature, it shows a greater morphological variability of the seafloor with respect to Lampedusa. On the other hand, BD and BDRS segmentations were largely overlapping for Lampedusa, (even if BDRS appears as more sensitive, see Fig. ESM3.3). This suggests that the use of BD segmentation is more suitable for regular and smoother seafloor without extensive variation in roughness and slope (such as observed in the application of Lacharité et al. 2017, on

a large shelf sector offshore Canada), while BDRS slightly outperforms BD in case of larger variability in the seafloor morphology. Starting from the results of BDRS segmentation and the acquired ground-truth data, the seabed maps of Linosa and Lampedusa have been proposed.

Seabed maps

Linosa

For Linosa, the seabed characteristics appears strongly dependent on the benthic habitat: both ROV investigations and grab samples showed, in fact, a prevalent and widespread bioclastic sedimentary cover on the seabed and the occurrence of very well-developed coralligenous habitats, with abundant rhodoliths and maërl beds. Therefore in order to create the seabed map of Linosa (at scale 1: 20 000), extending the information from ground-truth into areas with similar characteristics, the results of RSO-BIA segmentation (i.e. each majority class of the BDRS classification, Fig. 11b) were associated with benthoscape classes (sensu Lacharité et al. 2017), obtaining the following eight categories and corresponding characteristics (Fig. 13):

- *B—Bedrock*: homogeneous pattern of high backscatter, high roughness and variable slope. Locally the bedrock is colonized by seagrass and/or by photophilic algae (e.g. see Rov1 and 2 in Fig. 7).
- *VP—Volcaniclastic sand with *P. oceanica**: intermediate backscatter interrupted by elongated patches of high backscatter, intermediate roughness (due to presence of seagrass) and low slope. The seabed composition is characterized by volcaniclastic coarse sand and gravel (cobbles and pebbles), with scarce bioclastic sand fraction interspaced with maërl (see Rov8 and sample 10 in Fig. 5, sector 1).
- *VB—Volcaniclastic and Bioclastic sand*: high backscatter pattern, low roughness and low slope. Seabed composition characterized by volcaniclastic coarse sand with few bioclastic sand fraction interspaced with maërl (e.g. see sample 3 in Fig. 6, sector 2).
- *BV—Bioclastic and Volcaniclastic sand*: homogeneous pattern of high backscatter, intermediate roughness and high slope. Seabed composition characterized by maërl and bioclastic coarse sand with fewer volcaniclastic sand fractions (e.g. see ROV11 in Fig. 6, sector 3).
- *RM—Rhodolith and Maërl beds*: homogeneous pattern of medium/low backscatter, low roughness, low slope. The seabed composition is characterized by rhodolith and maërl beds and bioclastic coarse/medium sand (e.g. see ROV7 in Fig. 5, sector 2 and ROV4 in Fig. 8, sector 2).
- *RML—Rhodolith, Maërl and *Lythophyllum* beds*: homogeneous pattern of medium/low backscatter, low roughness, low slope. The seabed composition is characterized by rhodolith maërl and *Lythophyllum* beds that cover bioclastic medium/fine sand (e.g. see Rov14 in Fig. 5, sector 3 and Rov4 in Fig. 8, sector 2).
- *MB—Maërl and/or Bioclastic fine sand*: homogeneous pattern of low backscatter, intermediate roughness, high slope. The seabed composition is characterized by maërl and bioclastic fine sand (e.g. see Rov14 in Fig. 5, sector 3).
- *Bfs—Bioclastic fine sand*: homogeneous pattern of low backscatter, intermediate roughness, high slope. The seabed composition is mostly characterized by bioclastic fine sand (see sample 4 in Fig. 8, sector 2).

Moreover, since *P. oceanica* on rock is not recognizable in the segmentation procedures, but only through the video images (ROV1 and 2 in Fig. 7), further information on benthic habitat distribution (seagrasses) were manually added as overprinted symbols (*P. oceanica* on rock). To make the map more consistent, the same was done for the *P. oceanica* on sand even if this had been recognized in the segmentation (VP). Overall, it can be noted that the first facies of the benthoscape classification (“Bedrock” in Fig. 13) is common in the NW (“Secca di Tramontana”) and SE shallow-water areas, in correspondence of widely-eroded secondary volcanic edifices on the insular shelf, and in coastal areas around most of the island, as the prosecution of lava flows in shallow water. Volcaniclastic sand is abundant along the western shelf, where it is produced by erosion of tuff rings in the coastal area and reworked in submerged depositional terraces and is mixed with a bioclastic fraction. This fraction becomes more and more abundant downslope (below about 50 m depth) and showed scattered rhodoliths and lower grain size with increasing depth. Conversely, *P. oceanica* meadows on coarse sand are abundant on the inner insular shelf (first 30 m depth) all along the S flank of the island, above the thick and laterally continuous depositional terrace, while the frontal scarp of the terrace is covered by volcaniclastic and bioclastic coarse sand. Facies dominated by calcareous biogenic concretions (Rhodoliths and maërl) are widespread on the outer shelf areas (to the SW-S-SE and NW of the island), from about 60 m to about 100 m of depth, passing to bioclastic fine sand (with associated maërl) below that depth. The proposed benthoscape classification is still preliminary because it is based on a first integration of available data. Further ground-truth data are necessary to better characterize some acoustic facies not extensively sampled in this first survey, and related ecological systems.

Lampedusa

In order to create a seabed map for Lampedusa (at scale 1: 32 000), the interpretation of the RSOBIA shape file focused on BDRS majority classes locally checked through video inspections. Because no grab sampling is available here, the seabed was, in fact, mainly classified on the basis of its acoustic facies pattern (i.e. fine sediments exhibiting low backscatter, and coarse sediments corresponding to high backscatter) and the results of RSOBIA segmentation (majority classes of the BDRS classification, see “RSOBIA” section). So, eight main categories have been described and interpreted with respect to backscatter, roughness and slope characteristics to produce a preliminary benthoscape classification of Lampedusa (Fig. 14):

- *A—Speckled pattern of medium backscatter*: interrupted by homogeneous pattern of high backscatter. It is characterized by high roughness and intermediate slope. The substrate is mostly composed of bedrock and gravel (Video 1 of Fig. 9, sector 3), but in some sectors includes patches of *P. oceanica* (Fig. 9, sector 4).
- *B—Homogeneous pattern of high backscatter*: characterized by low roughness and low slope. It presumably represents a substratum with coarse-grained sediment.
- *C—Homogeneous pattern of medium/high backscatter*: low roughness and variable slope. It presumably represents a substratum with coarse/medium sand, generally without any evidence of seagrasses (Video 5 of Fig. 10, sector3).
- *D—Speckled pattern of intermediate backscatter*: interrupted by circular and/or elongated pattern of high backscatter, intermediate roughness and slope. This class include *P. oceanica* meadows ‘on matte’ (see ESM2 and Fig. 9, sector 5) with holes at which are almost always filled with coarse sand. The kind of sediment below the seagrass cannot be constrained without any grab sampling.
- *E—Speckled pattern of low backscatter*: interrupted by circular and/or elongated pattern of high backscatter, intermediate roughness and low slope. This class include dense *P. oceanica* meadows interspaced with coarse sand (Fig. 10, sector 1 and video 7 of sector2). An exception to this is witnessed by Video 2 of Fig. 9 which showed a sandy seabed covered by *Cymodocea nodosa*. Future samples will allow to better define the type of sediment.

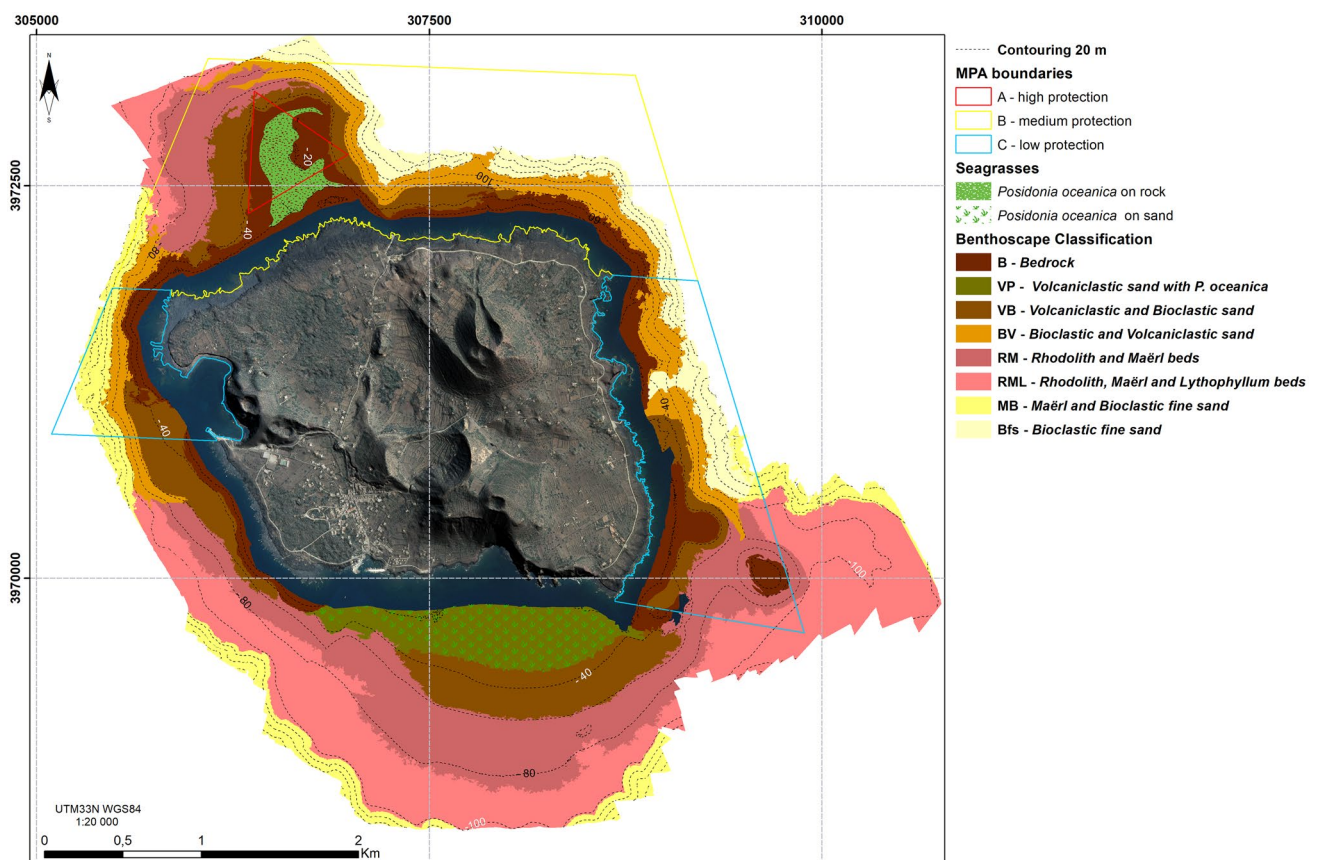


Fig. 13 Benthoscape classification of Linosa Island obtained with the interpretation of RSOBIA-BDRS segmentation; Seagrasses on rock and on sand have been added manually as over printed symbols. Also

the areas boundaries of the MPA of Linosa were added in map, where the level of protection decrease from area A to area C (see <http://www.minambiente.it/pagina/area-marina-protetta-isole-pelagie>)

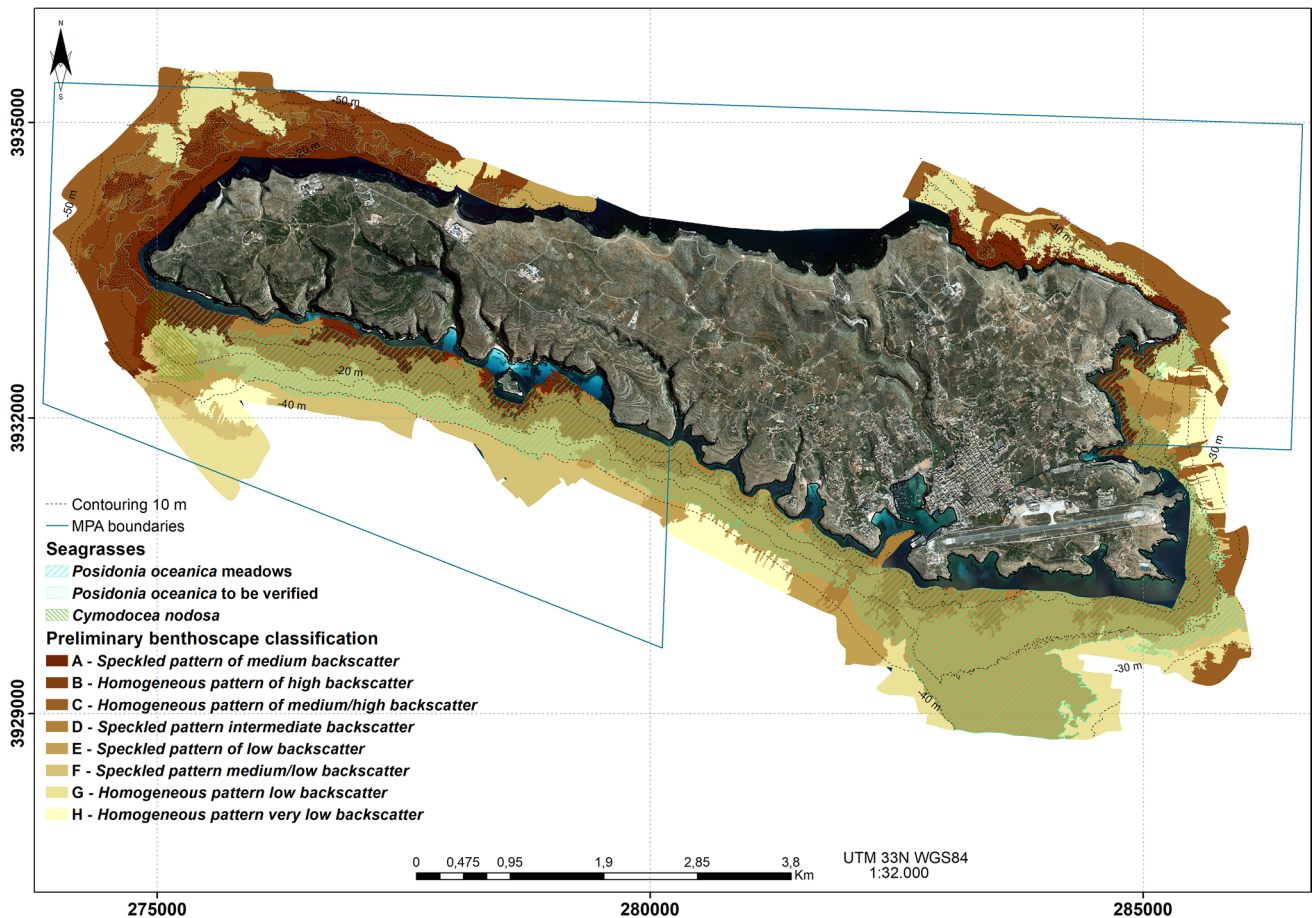


Fig. 14 Preliminary benthoscape classification of Lampedusa Island obtained with the interpretation of RSOBIA-BDRS segmentation. Seagrasses have been added manually as over printed symbols. Also the areas boundaries of the MPA of Lampedusa were added in map

- *F*—*Speckled pattern of medium/low backscatter*: intermediate/low roughness and slope. This acoustic facies is the most difficult to classify because it includes both areas with rock and *Posidonia oceanica* (Video 6 of Fig. 10, sector 4), and the sector to the south of the island where the lower limit of the *P. oceanica* meadows occurs. *Posidonia* on ‘matte’ here gradually thins out, both in density of leaves and height (Video 4 of Fig. 9, sector 5). Finally, it includes the dune sector (Video 3 of Fig. 9, sector 1), likely composed of medium-fine sand.
- *G*—*Homogeneous pattern of low backscatter*: low roughness and slope. It likely represents a substratum with fine grained sediment, without any evidence of seagrasses. This class also encloses the dune field sector (Video 3 of Fig. 9, sector 1)
- *H*—*Homogeneous pattern of very low backscatter*: (very high absorption), low roughness and slope. It presumably represents a substratum with very fine grained sediment and silt, but in some cases it includes sectors previously classified by Tonielli et al. 2016 as *P. oceanica* in patches.

From interpretations given in “**Lampedusa**” section and map of Fig. 14 it appears that the shallow-water areas in most of the coastal strip, in particular along the W and NE flanks of the island are characterized by bedrock covered with very coarse and heterogeneous sediments. A sandy seabed (from coarse-medium size) was present at very shallow depth along the S flank of the island and, in general, at increasing depth, gradual shifting to finer-size sand. Again, further information on benthic habitat distribution (seagrasses) have been manually added as overprint layers, consistent with video inspections (Fig. 14):

- *Posidonia oceanica* meadows
- *Posidonia oceanica* to be verified (this area falls under “*Posidonia oceanica* in patch” according the classification of Tonielli et al. 2016)
- *Cymodocea nodosa*

Discussion

This paper merges together geomorphological, sedimentological and habitat observations at the Pelagic Islands of Lampedusa and Linosa, resulting in an integrated, multipurpose seabed mapping. To this aim we applied the RSOBIA methodology and tested it: (1) on different geological substrata (volcanic and sedimentary), (2) on very heterogeneous lithological and morpho-sedimentary conditions (flat or gentle-sloping sea bed, articulated seabed with scarps, volcanic outcrops or loose sediment, erosive or depositional features) and (3) over a differently-colonized seafloor. In particular, we found that among the resulting output (shape files) of RSOBIA, the BDRS segmentation is the most suitable to build the final benthoscape map. We did not adopt a manual re-classification based on uncertainties in membership values to individual classes—especially at the boundaries between coverages—as carried out by Lacharité et al. (2017). However, it is important to keep in mind the role of the operator, that remains crucial for the recognition of some specific acoustic facies, and the need of abundant ground-truth data to characterize acoustic facies and to support interpretations. As an example of this, at Linosa, the high density of coralligenous habitat (i.e. maërl, rhodoliths and *Lhytophyllum*) causes a saturation of the backscatter signal to intermediate values, making the seabed classification difficult through the sole use of acoustic mosaic. In similar cases, such as at Palinuro Seamount (central Mediterranean; Innangi et al. 2016), or western Sardinia (De Falco et al. 2010) and northern Tyrrhenian sector of Basilicata (Innangi et al. 2015) the presence of *P. oceanica* meadows (or other biogenic components) on the seabed tends to reduce the value of backscatter strength, showing an increase in absorption and giving rise to a possible mismatch between the acoustic facies of medium and/or coarse sands. Thus, the integration of ground-truth data and the manual processing is required for adequate interpretation of the acoustic pattern derived from the RSOBIA output. In the southern shallow-water sector of Linosa, for instance, where the low seabed slope and superficial currents allow a luxuriant growth of coralline environment, BDRS segmentation appears more dependent on bathymetric changes than on backscatter variations and it underestimates the variability in the benthic habitat. Indeed, by ROV video images it can be observed that the distribution of *Lhytophyllum* is present here in a range of depths varying between 100 and 85 meters, while rhodolith beds seem to find their ideal environment between 90 and 60 meters. The distribution of maërl (composed of spheroidal, discoidal and ellipsoidal shape branched classes, Peña and Bárbara 2009) is also widely common around the island. The only well-distinguished facies according to both bathymetry and backscatter data (well recognized also by BDRS segmentation as majority class 2, Fig. 11b) is the *P.*

oceanica meadow on the southern part of the island (depth between –20 m to –36 m) lying on a coarse-sand substrate (characterized by high backscatter, i.e. darker area on the acoustic mosaic). The occurrence of *P. oceanica* on rock, on the other hand is not distinguishable without direct observation, unless it is very dense, both in Linosa and in Lampedusa. Furthermore, where volcanoclastic sands prevail over bioclastic sands and maërl, the backscatter signal is overbearing in the BDRS segmentation (i.e. majority class 6, Fig. 11b), as it occurs for fine sand without maërl (i.e. majority 1, Fig. 11b). At Lampedusa, in absence of grain-size and lithological information, the BDRS segmentation allowed a preliminary mapping of the seabed typologies, based on morpho-acoustic data, and will need to be implemented with further investigations. The map obtained through the object-based method was then integrated with indications of the *P. oceanica* meadows extension, obtained through video image analysis and previous interpretation of the morpho-acoustic data (according to Tonielli et al. 2016). To conclude, the combination of RSOBIA segmentation, ground-truth data and manual processing provide a suitable approach for seabed mapping and for a better understanding of the fine-scale distribution of benthic habitats. This approach should be supported by further investigations and sampling of the Pelagic Islands, in order to have more robust interpretations.

Conclusions

The surveys carried out around the Pelagic islands revealed a very rich ecosystem, both for the development of *P. oceanica* and for the presence of coralligenous habitats, confirming what had been previously proposed by predictive modeling for this area (Martin et al. 2014). In particular, the morphological setting of Lampedusa, with less steep submarine flanks than Linosa and with a sedimentary substratum, favors the development of *P. oceanica* meadows. The volcanic seabed at Linosa, on the other hand, proved to be more suitable for coralligenous environments, characterized by pristine coralligenous habitats that need to be preserved. The reasons for such a highly productive environment around this island may be several, e.g. the presence of upwelling currents, or its volcanic nature rich in nutrients, or the low human impact that still prevails here. Our first seabed mapping supports the enlargement of the Marine Protected Area of Linosa, including the coralligenous habitat identified on this island and that represents a unique heritage for the Mediterranean Sea. In conclusion on the seabed of Linosa and Lampedusa three important ecosystems have been identified (i.e. *P. oceanica*, coralligenous assemblages and maërl). These areas have been recognized as VMEs (Vulnerable Marine Ecosystems) by the EU and other official environmental commissions (<http://www.fao.org/in-action/>

vulnerable-marine-ecosystems/en/; e.g. Francour et al. 2006; Bensch et al. 2009; OCEANA 2009; Bernal 2016). The seabed classification and the recognition of its priority habitats are basic elements for a proper management of this Marine Protected Area (e.g. Ehrhold et al. 2006; Bracchi et al. 2015; Le Bas and Huvenne 2009; Micallef et al. 2012). Accordingly, as can be seen on the maps, a good extension of *P. oceanica* (both for Linosa the for Lampedusa) and a rich coralligenous environment (for Linosa) has been found out the boundaries of the MPA. Thus, our first seabed mapping supports the enlargement of the Marine Protected Area of Linosa, and suggests the possibility that these boundaries should be modified, both as extension and as level of protection. The capability to classify the seabed in an automated or semi-automated manner could guarantee the objectivity and repeatability of the application over time (e.g. Lucieer 2008; Lucieer and Lamarche 2011; Huang et al. 2014; Ismail et al. 2015; Lacharité et al. 2017). The use of RSOBIA (integrated by geomorphological, sedimentological and habitat observations) proved to be a sound method for this purpose, allowing an initial seabed classification regardless of the availability of grain size information (as at Lampedusa) or of the clarity of the acoustic facies (as at Linosa).

Acknowledgements We thank Simone D’Ippolito, the captain of the M/B ‘Risal’, for the help and continuous support during all the operations of data acquisition. Thanks to the crew of the R/V ‘Minerva Uno’, for all the support during board and research operations. The authors wish to thank Sergio Monteleone and Patricia Scaffani for their comments to the first draft of the manuscript.

Funding This study benefited from contribution of the project “Implementation of research activity and monitoring around Pelagic Islands Marine Protected Area”, within the project “CAmBiA – Contabilità Ambientale e Bilancio Ambientale” funded by the Ministry of the Environment and Protection of Land and Sea (MATTM – Ministero dell’Ambiente e della Tutela del Territorio e del Mare), directive n° 5135 of march 2015. This study also benefited from the contribution of the RITMARE Flagship Project, funded by Ministry of Education, University and Research (MIUR – Ministero dell’Istruzione dell’Università e della Ricerca) [NRP 2011–2013].

References

- Agardy MT (1994) Advances in marine conservation: the role of marine protected areas. *Trends Ecol Evol* 9:267–270. [https://doi.org/10.1016/0169-5347\(94\)90297-6](https://doi.org/10.1016/0169-5347(94)90297-6)
- Agnesi S, Annunziatellis A, Casese ML et al (2009) Analysis on the coralligenous assemblages in the Mediterranean Sea: a review of the current state of knowledge in support of future investigations. In: Proceedings of the 1st Mediterranean symposium on the conservation of the coralligenous and other calcareous bio-concretions. C. Pergent-Martini & M. Bricchet (Eds). UNEP-MAP RAC/SPA (Tabarka, 15–16 January 2009). Tunis, RAC/SPA publication
- Argnani A (1990) The strait of sicily rift zone: foreland deformation related to the evolution of a back-arc basin. *J Geodyn* 12:311–331. [https://doi.org/10.1016/0264-3707\(90\)90028-S](https://doi.org/10.1016/0264-3707(90)90028-S)
- Astraldi M, Gasparini GP, Gervasio L, Salusti E (2001) Dense water dynamics along the strait of sicily (Mediterranean Sea). *J Phys Oceanogr* 31:3457–3475. [https://doi.org/10.1175/1520-0485\(2001\)031%3C3457:DWDATS%3E2.0.CO;2](https://doi.org/10.1175/1520-0485(2001)031%3C3457:DWDATS%3E2.0.CO;2)
- Ballesteros E (2006) Mediterranean coralligenous assemblages: a synthesis of present knowledge. *Oceanogr Mar Biol* 44:123–195
- Barbera C, Bordehore C, Borg JA et al (2003) Conservation and management of northeast Atlantic and Mediterranean maerl beds. *Aquat Conserv Mar Freshw Ecosyst* 13:65–76. <https://doi.org/10.1002/aqc.569>
- Bensch A, Gianni M, Greboval D et al (2009) Worldwide review of bottom fisheries in the high seas. *FAO Fish Tech Pap* 552:145
- Bentrem FW, Avera WE, Sample J (2006) Estimating surface sediments using multibeam sonar—acoustic backscatter processing for characterization and mapping of the ocean bottom. *Sea Technol* 47:37
- Bernal M (2016) Management of deep sea fisheries and protection of vulnerable marine ecosystems in the Mediterranean Sea. In: The General Fisheries Commission for the Mediterranean, FAO—GFCM Fishery Resources Officer
- Biondo M, Bartholomä A (2017) A multivariate analytical method to characterize sediment attributes from high-frequency acoustic backscatter and ground-truthing data (Jade Bay, German North Sea coast). *Cont Shelf Res* 138:65–80. <https://doi.org/10.1016/j.csr.2016.12.011>
- Birkett DA, Maggs C, Drig MJ (1998) An overview of dynamics and sensitivity characteristics for conservation management of marine SACs. V:1–117
- Blaschke T (2010) Object based image analysis for remote sensing. *ISPRS J Photogramm Remote Sens* 65:2–16. <https://doi.org/10.1016/j.isprsjprs.2009.06.004>
- Bonacorsi M, Pergent-Martini C, Clabaut P, Pergent G (2012) Coral-ligenous “atolls”: discovery of a new morphotype in the Western Mediterranean Sea. *Comptes Rendus Biol* 335:668–672. <https://doi.org/10.1016/j.crvi.2012.10.005>
- Bracchi V, Savini A, Marchese F et al (2015) Coralligenous habitat in the Mediterranean Sea: a geomorphological description from remote data. *Ital J Geosci* 134:32–40. <https://doi.org/10.33011/IJG.2014.16>
- Bracchi VA, Basso D, Marchese F et al (2017) Coralligenous morphotypes on subhorizontal substrate: a new categorization. *Cont Shelf Res* 144:10–20. <https://doi.org/10.1016/j.csr.2017.06.005>
- Briggs KB, Tang D, Williams KL (2002) Characterization of interface roughness of rippled sand off fort Walton Beach, Florida. *IEEE J Ocean Eng* 27:505–514. <https://doi.org/10.1109/JOE.2002.1040934>
- Brown CJ, Blondel P (2009) Developments in the application of multibeam sonar backscatter for seafloor habitat mapping. *Appl Acoust* 70:1242–1247. <https://doi.org/10.1016/j.apacoust.2008.08.004>
- Brown CJ, Smith SJ, Lawton P, Anderson JT (2011) Benthic habitat mapping: a review of progress towards improved understanding of the spatial ecology of the seafloor using acoustic techniques. *Estuar Coast Shelf Sci* 92:502–520. <https://doi.org/10.1016/j.ecss.2011.02.007>
- Bunting P, Clewley D, Lucas RM, Gillingham S (2014) The remote sensing and GIS software library (RSGISLib). *Comput Geosci* 62:216–226. <https://doi.org/10.1016/j.cageo.2013.08.007>
- Calanchi N, Colantoni P, Rossi PL et al (1989) The strait of sicily continental rift systems: physiography and petrochemistry of the submarine volcanic centres. *Mar Geol* 87:55–83. [https://doi.org/10.1016/0025-3227\(89\)90145-X](https://doi.org/10.1016/0025-3227(89)90145-X)
- Chiocci FL, D’Angelo S, Romagnoli C (2004) Atlas of submerged depositional terraces along the Italian coast. Roma
- Civile D, Lodolo E, Accettella D et al (2010) The Pantelleria graben (Sicily Channel, Central Mediterranean): an example of intra-plate “passive” rift. *Tectonophysics* 490:173–183. <https://doi.org/10.1016/j.tecto.2010.05.008>

- Collier JS, Brown CJ (2005) Correlation of sidescan backscatter with grain size distribution of surficial seabed sediments. *Mar Geol* 214:431–449. <https://doi.org/10.1016/j.margeo.2004.11.011>
- Dartnell P, Gardner JV (2004) Predicting seafloor facies from multi-beam bathymetry and backscatter data. *Photogramm Eng Remote Sens* 70:1081–1091. <https://doi.org/10.14358/PERS.70.9.1081>
- De Falco G, Tonielli R, Di Martino G et al (2010) Relationships between multibeam backscatter, sediment grain size and *Posidonia oceanica* seagrass distribution. *Cont Shelf Res* 30:1941–1950. <https://doi.org/10.1016/j.csr.2010.09.006>
- Di Geronimo R, Giaccone G (1994) Le alghe calcaree nel detritico costiero di Lampedusa (Isole Pelagie). *Boll Accad Gioenia Sci Nat Catania* 27:5–25
- Di Martino G, Innangi S, Felsani M et al (2015) Acquisizione dati morfo-batimetrici: convenzione Isole Pelagie per il monitoraggio della prateria a *Posidonia oceanica*. Technical Report, IAMC-CNR, p. 12. SOLAR. <http://eprints.bice.rm.cnr.it/11261/>
- Diesing M, Green SL, Stephens D et al (2014) Mapping seabed sediments: comparison of manual, geostatistical, object-based image analysis and machine learning approaches. *Cont Shelf Res* 84:107–119. <https://doi.org/10.1016/j.csr.2014.05.004>
- Ehrhold A, Hamon D, Guillaumont B (2006) The REBENT monitoring network, a spatially integrated, acoustic approach to surveying nearshore macrobenthic habitats: application to the Bay of Concarneau (South Brittany, France). *ICES J Mar Sci* 63:1604–1615. <https://doi.org/10.1016/j.icesjms.2006.06.010>
- Ferrini VL, Flood RD (2006) The effects of fine-scale surface roughness and grain size on 300 kHz multibeam backscatter intensity in sandy marine sedimentary environments. *Mar Geol* 228:153–172. <https://doi.org/10.1016/j.margeo.2005.11.010>
- Fledermaus User Manual (2016) QPS and Saab Group. <https://confluence.qps.nl/fm780>
- Folk RL (1980) Petrology of sedimentary rocks. 170. Hemphill Publ Company, Austin. <https://doi.org/10.1017/CBO9781107415324.004>
- Fonseca L, Mayer L (2007) Remote estimation of surficial seafloor properties through the application angular range analysis to multibeam sonar data. *Mar Geophys Res* 28:119–126. <https://doi.org/10.1007/s11001-007-9019-4>
- Fonseca L, Brown C, Calder B et al (2009) Angular range analysis of acoustic themes from Stanton Banks Ireland: a link between visual interpretation and multibeam echosounder angular signatures. *Appl Acoust* 70:1298–1304. <https://doi.org/10.1016/j.apacoust.2008.09.008>
- Francour P, Magréau JF, Mannoni AP et al (2006) Management guide for Marine Protected Areas of the Mediterranean sea, permanent ecological moorings. Univ Nice-Sophia Antip Parc Natl Port-Cros, Nice 68 pp
- Giardina F, De Rubeis P (2012) Analisi della prateria a *Posidonia oceanica* (L.) Delile (Najadales, Potamogetonaceae) dell'isola di Lampedusa (AMP "Isole Pelagie", Canale di Sicilia). *Boll Accad Gioenia di Sci Nat di Catania* 45:651–664
- Gobert S, Cambridge M, Velimirov B et al (2006) Biology of *Posidonia*. In: Larum A, Orth R, Duarte C (eds) *Seagrasses: biology, ecology and conservation*. Springer, Berlin. pp 387–408
- Goff JA, Kraft BJ, Mayer LA et al (2004) Seabed characterization on the New Jersey middle and outer shelf: correlatability and spatial variability of seafloor sediment properties. *Mar Geol* 209:147–172. <https://doi.org/10.1016/j.margeo.2004.05.030>
- Grasso M, Pedley HM (1985) The Pelagian Islands: a new geological interpretation from sedimentological and tectonic studies and its bearing on the evolution of the Central Mediterranean Sea (Pelagian Block). *Geol Rom* 24:13–34
- Grasso M, Pedley HM (1988) Carta geologica dell'isola di Lampedusa. Isole Pelagie, Mediterraneo Centrale) 1/10,000. Cartogr SELCA, Florence
- Grasso M, Lanzafame G, Rossi PL et al (1991) Volcanic evolution of the island of Linosa, strait of Sicily. *Geol Soc Italy Mem* 47:509–525
- Guidetti P, Milazzo M, Bussotti S et al (2008) Italian marine reserve effectiveness: does enforcement matter? *Biol Conserv* 141:699–709. <https://doi.org/10.1016/j.biocon.2007.12.013>
- Hemminga MA, Duarte CM (2000) *Seagrass ecology*. Cambridge University Press, Cambridge. p 298.
- Hillman JIT, Lamarche G, Pallentin A et al (2017) Validation of automated supervised segmentation of multibeam backscatter data from the Chatham Rise, New Zealand. *Mar Geophys Res* 0:1–23. <https://doi.org/10.1007/s11001-016-9297-9>
- Huang Z, Siwabessy J, Nichol SL, Brooke BP (2014) Predictive mapping of seabed substrata using high-resolution multibeam sonar data: a case study from a shelf with complex geomorphology. *Mar Geol* 357:37–52. <https://doi.org/10.1016/j.margeo.2014.07.012>
- Ierodiaconou D, Schimel ACG, Kennedy D et al (2018) Combining pixel and object based image analysis of ultra-high resolution multibeam bathymetry and backscatter for habitat mapping in shallow marine waters. *Mar Geophys Res* 39:271–288. <https://doi.org/10.1007/s11001-017-9338-z>
- Innangi S, Tonielli R (2017) Relazione finale della Campagna Oceanografica "Linosa." Technical Report, IAMC-CNR, p 20, SOLAR. <http://eprints.bice.rm.cnr.it/id/eprint/15783>
- Innangi S, Barra M, Brando A et al (2008) Construction of the thematic maps of the seabed along the Lucanian Tyrrhenian Coast of Maratea (PZ). *Rend Online Soc Geol Ital* 3:476–477
- Innangi S, Barra M, Di Martino G et al (2015) Reson SeaBat 8125 backscatter data as a tool for seabed characterization (Central Mediterranean, Southern Italy): results from different processing approaches. *Appl Acoust* 87:109–122. <https://doi.org/10.1016/j.apacoust.2014.06.014>
- Innangi S, Passaro S, Tonielli R et al (2016) Seafloor mapping using high-resolution multibeam backscatter: The Palinuro Seamount (Eastern Tyrrhenian Sea). *J Maps* 12:736–746. <https://doi.org/10.1080/17445647.2015.1071719>
- Ismail K, Huvenne VAI, Masson DG (2015) Objective automated classification technique for marine landscape mapping in submarine canyons. *Mar Geol* 362:17–32. <https://doi.org/10.1016/j.margeo.2015.01.006>
- Jameson SC, Tupper MH, Ridley JM (2002) The three screen doors: can marine "protected" areas be effective? *Mar Pollut Bull* 44:1177–1183. [https://doi.org/10.1016/S0025-326X\(02\)00258-8](https://doi.org/10.1016/S0025-326X(02)00258-8)
- Karoui I, Fablet R, Boucher JM, Augustin JM (2009) Seabed segmentation using optimized statistics of sonar textures. *IEEE Trans Geosci Remote Sens* 47:1621–1631. <https://doi.org/10.1109/TGRS.2008.2006362>
- Kostylev V, Todd B, Fader G et al (2001) Benthic habitat mapping on the Scotian Shelf based on multibeam bathymetry, surficial geology and sea floor photographs. *Mar Ecol Prog Ser* 219:121–137
- Laborel J (1961) Le concrétionnement algal "coralligène" et son importance géomorphologique en Méditerranée. *Rec Trav Stat Mar Endoume* 23:37–60
- Laborel J (1987) Marine biogenic constructions in the Mediterranean. *Sci Rep Port-Cros Natl Park* 13:97–126
- Lacharité M, Brown CJ, Gazzola V (2017) Multisource multibeam backscatter data: developing a strategy for the production of benthic habitat maps using semi-automated seafloor classification methods. *Mar Geophys Res* 39:307–322. <https://doi.org/10.1007/s11001-017-9331-6>
- Lanti E, Lanzafame G, Rossi PL et al (1988) Vulcanesimo e tettonica nel Canale di Sicilia: l'isola di Linosa. *Miner Petrogr Acta* 31:69–93

- Lanzafame G, Rossi PL, Tranne CA, Lanti E (1994) Carta geologica dell'isola di Linosa 1: 5000. SELCA
- Le Bas T (2016) RSOBIA—a new OBIA toolbar and toolbox in ArcMap 10.x for segmentation and classification. In: Kerle N, Gerke M, Lefevre S (eds) GEOBIA 2016: Solutions and Synergies. University of Twente Faculty of Geo-Information and Earth Observation, Twente, p 4
- Le Bas TP, Huvenne VAI (2009) Acquisition and processing of backscatter data for habitat mapping—comparison of multibeam and sidescan systems. *Appl Acoust* 70:1248–1257. <https://doi.org/10.1016/j.apacoust.2008.07.010>
- Lentini F, Carbone S, Catalano S, Grasso M (1995) Principali lineamenti strutturali della Sicilia nord-orientale. *Stud Geol Camerti* 2:319–929
- Li M, Zang S, Zhang B et al (2014) A review of remote sensing image classification techniques: the role of Spatio-contextual information. *Eur J Remote Sens* 47:389–411. <https://doi.org/10.5721/EuJRS20144723>
- Lo Iacono C, Gràcia E, Diez S et al (2008) Seafloor characterization and backscatter variability of the Almería Margin (Alboran Sea, SW Mediterranean) based on high-resolution acoustic data. *Mar Geol* 250:1–18. <https://doi.org/10.1016/j.margeo.2007.11.004>
- Lucieer VL (2008) Object-oriented classification of sidescan sonar data for mapping benthic marine habitats. *Int J Remote Sens* 29:905–921. <https://doi.org/10.1080/01431160701311309>
- Lucieer V, Lamarche G (2011) Unsupervised fuzzy classification and object-based image analysis of multibeam data to map deep water substrates, Cook Strait, New Zealand. *Cont Shelf Res* 31:1236–1247. <https://doi.org/10.1016/j.csr.2011.04.016>
- Mallace D (2012) QPS- Fledermaus Workshop- FMGeocoder Webinar. 1–49
- Martin CS, Giannoulaki M, De Leo F et al (2014) Coralligenous and maërl habitats: predictive modelling to identify their spatial distributions across the Mediterranean Sea. *Sci Rep* 4:1–9. <https://doi.org/10.1038/srep05073>
- Micallef A, Le Bas TP, Huvenne VAI et al (2012) A multi-method approach for benthic habitat mapping of shallow coastal areas with high-resolution multibeam data. *Cont Shelf Res* 39–40:14–26. <https://doi.org/10.1016/j.csr.2012.03.008>
- Montealeale Gavazzi G, Madricardo F, Janowski L et al (2016) Evaluation of seabed mapping methods for fine-scale classification of extremely shallow benthic habitats—application to the Venice Lagoon, Italy. *Estuar Coast Shelf Sci* 170:45–60. <https://doi.org/10.1016/j.ecss.2015.12.014>
- OCEANA (2009) Developing a list of Vulnerable Marine Ecosystems. In: 40th session of the General Fisheries Commission for the Mediterranean Mediterranean VMEs: diverse, fragile habitats that support fisheries
- Parnum I, Gavrilov A, Siwabessy P, Duncan A (2005) The effect of incident angle on statistical variation of backscatter measured using a high-frequency multibeam sonar. In: Proceedings of ACOUSTICS 2005, Busselton, Western Australia, 9–11 November, pp 433–438
- Peña V, Bárbara I (2009) Distribution of the Galician maërl beds and their shape classes (Atlantic Iberian Peninsula): proposal of areas in future conservation actions. *Cah Biol Mar* 50:353–368
- Pérès JM, Picard J (1964) Nouveau manuel de bionomie benthique de la mer Méditerranée. Recl des Trav la Stn Mar d'Endoume 31:1–131
- Pettijohn FJ, Potter PE, Siever R (1987) Sand and sandstone. *Soil Sci* 117:130
- Pieraccini M, Coppa S, De Lucia GA (2016) Beyond marine paper parks? Regulation theory to assess and address environmental non-compliance. *Aquat Conserv Mar Freshw Ecosyst*. <https://doi.org/10.1002/aqc.2632>
- Pomeroy RS, Watson LM, Parks JE, Cid GA (2005) How is your MPA doing? A methodology for evaluating the management effectiveness of marine protected areas. *Ocean Coast Manag* 48:485–502. <https://doi.org/10.1016/j.ocecoaman.2005.05.004>
- Poulain P-M, Menna M, Mauri E (2012) Surface geostrophic circulation of the Mediterranean Sea derived from drifter and satellite altimeter data. *J Phys Oceanogr* 42:973–990. <https://doi.org/10.1175/JPO-D-11-0159.1>
- Romagnoli C (2004) Submerged depositional terraces around Linosa Island (Sicily Channel). In: APAT - Memorie descrittive della Carta Geologica D'Italia. pp 71–74
- Sartoretto S (1994) Structure et dynamique d'un nouveau type de bioconstruction à Mesophyllum lichenoides (Ellis) Lemoine (Coralinales, Rhodophyta). *Comptes rendus l'Académie des Sci Série 3 Sci la vie* 317:156–160
- Stewart WK, Chu D, Malik S et al (1994) Quantitative seafloor characterization using a bathymetric sidescan sonar. *IEEE J Ocean Eng* 19:599–610. <https://doi.org/10.1109/48.338396>
- Sutherland T, Galloway J, Loschiavo R et al (2007) Calibration techniques and sampling resolution requirements for groundtruthing multibeam acoustic backscatter (EM3000) and QTC VIEW™ classification technology. *Estuar Coast Shelf Sci* 75:447–458. <https://doi.org/10.1016/j.ecss.2007.05.045>
- Tonielli R, Innangi S, Budillon F et al (2016) Distribution of *Posidonia oceanica* (L.) Delile meadows around Lampedusa Island (Strait of Sicily, Italy). *J Maps* 12:249–260. <https://doi.org/10.1080/17445647.2016.1195298>
- Truffarelli C, Belluscio A, Criscioli A, Ardizzone GD (2012) Interpretation of Sonar Images in the *Posidonia oceanica* cartography. Sonograms analysis and description. *Biol Mar Mediterr* 19:84–91
- UNEP-MAP-RAC, SPA (2008) Action plan for the conservation of the coralligenous and other calcareous bio-concretions in the Mediterranean Sea. UNEP MAP RAC-SPA publ, Tunis
- UNEP-MAP-RAC, SPA (2015) Sicily Channel/Tunisian Plateau: Topography, circulation and their effects on biological component. UNITED NATIONS Environ Program Mediterr ACTION PLAN, Tunis
- Wagstaff K, Cardie C, Rogers S, Schroedl S (2001) Constrained K-means clustering with background knowledge. *Int Conf Mach Learn* 577–584. <https://doi.org/10.1109/TPAMI.2002.1017616>
- Wright DJ, Pendleton M, Boulware J et al (2012) ArcGIS Benthic Terrain Modeler (BTM), v. 3.0, Environmental Systems Research Institute, NOAA Coastal Services Center, Massachusetts Office of Coastal Zone Management. esriurl.com/5754